UNIVERSIDADE DE LISBOA
FACULDADE DE CIÊNCIAS
DEPARTAMENTO QUÍMICA E BIOQUÍMICA

Oxidative stress response enzymes: unravelling catalytic determinants through natural and site directed mutants

Diogo Salazar Diniz

Mestrado em Bioquímica
Especialização em Bioquímica Médica

Dissertação orientada por:
Miguel Teixeira
Fernando Antunes

2021

UNIVERSIDADE DE LISBOA
FACULDADE DE CIÊNCIAS
DEPARTAMENTO QUÍMICA E BIOQUÍMICA

Oxidative stress response enzymes: unravelling catalytic determinants through natural and site directed mutants

Diogo Salazar Diniz

Mestrado em Bioquímica
Especialização em Bioquímica Médica

Dissertação orientada por:
Miguel Teixeira
Fernando Antunes

I. Acknowledgments

Gostaria de agradecer a todas as pessoas que me ajudaram a concluir esta etapa do meu percurso académico.

Primeiramente, gostaria de agradecer ao meu Orientador, o Professor Miguel Teixeira, pela oportunidade de integrar o seu grupo e por se ter mostrado sempre disponível para me ajudar. Em particular, gostaria de lhe agradecer por me ter concedido o seu gabinete para a redação desta dissertação, numa altura em que, devido à pandemia, as bibliotecas e cafés se encontravam encerrados.

Um grande agradecimento ao Dr. Filipe Folgosa, que apenas por motivos de logística não é o meu Coorientador oficial. Em primeiro lugar, obrigado pela enorme paciência e capacidade que demonstrou ter para me ensinar e orientar durante este período. A dedicação e disponibilidade que sempre mostrou, apesar do excesso de trabalho que tem, sempre! Pela orientação que se revelou essencial para este trabalho. Por último, mas não menos importante, pelas risadas e boa disposição que proporcionou com muitas histórias, algumas com espiões, outras com engenheiras, e todas com uma moral no final.

Ao meu orientador interno, o Professor Fernando Antunes pela disponibilidade e amabilidade.

Aos meus colegas de laboratório, Jéssica, Susana, Maria, Bruno e Silviya, pelo apoio que me sempre me deram, pela descontração e chamadas de atenção (Maria…). Muito obrigado pela ajuda que me deram do início ao fim, especial obrigado ao Bruno pelos trabalhos "rápidos" na cristalografia e à Jéssica minha companheira de intervalos.

Às minhas colegas Maria Firmino e Vanessa Costa que também vieram da FCUL, pelos almoços, lanches e trocas de experiências nesta fase.

A todas as pessoas que conheci e criei laços no ITQB durante esta fase, tanto antes como durante a pandemia, nos convívios quando eram realizados e mais tarde no voluntariado de Covid-19. Agradecimento especial ao Dr. Américo Duarte pela boa disposição quando vou chatear o Dr. Filipe e pela disponibilidade e ajuda que demonstrou mesmo não sendo parte do mesmo grupo. E à Cláudia pelo apoio e companhia na fase final de escrita do processo.

Aos meus amigos: Carréu, Fábio, Joana, Ayrton, Margarida, Xico, Tiago, Sara e Carl Ravinas. Pelas noitadas sem dormir, apoio incondicional que sempre me deram, cabeçadas sempre que necessário e pelas dores de costas que me dão! The Dean!

À minha família que sempre me apoiou e deu tudo o precisava para concluir esta fase. À minha Mãe, Pai, irmã e Avó, sendo as pessoas mais próximas. A todos os meus tios, tia e amigos próximos da família pelo carinho.

II. Abbreviations and Symbols

Af	*Archaeoglobus fulgidus*
BSA	Bovine Serum Albumin
Dfx	Desulfoferrodoxin
Dx	Desulforedoxin
E. coli	*Escherichia coli*
EPR	Electron Paramagnetic Resonance
ICP-AES	Inductively Coupled Plasma Atomic Emission Spectroscopy
IPTG	Isopropyl β-D-1-Thiogalactopyranoside
LB	Lysogeny Broth
Kc	*Korarchaeum cryptofilum*
M9	Minimum Salts Medium
NBT	Nitrobluetetrazolium
Nlr	Neelaredoxin
ROS	Reactive Oxygen Species
SDS-PAGE	Sodium Dodecyl Sulphate-Polyacrylamide Gel Electrophoresis
SOD	Superoxide dismutase
SOR	Superoxide Reductase
WT	Wild Type

III. Abstract

Superoxide reductases (SOR) are non-heme iron enzymes that can have one (1Fe-SOR) or two (2Fe-SOR) iron atoms and are capable to catalyse the one-electron reduction of $O_2^{\bullet -}$, to hydrogen peroxide. In 2Fe-SORs, the iron atoms, are present in two different centres, the desulforedoxin and the neelaredoxin centre, or centre I and II respectively. In the neelaredoxin centre, which is the catalytic centre in SORs, the iron atom is coordinated by four equatorial histidines and a fifth axial cysteine-ligand. On the other hand, in the desulforedoxin centre, which is similar to the *D. gigas* desulforedoxin, the iron is coordinated by the sulphur atoms from the four cysteine ligands, with the binding motif $CX_2CX_{15}CC$.

From the amino acid sequence analysis, *Korarchaeum cryptofilum* SOR is predicted to be a 2Fe-SOR, but one of the ligand histidines is substituted by one serine, raising the question of whether this protein is able to bind iron at the centre II. Besides this difference in the catalytic centre, *Kc* SOR also has an extra domain in the C-terminal region of the protein. The role of this domain is still unknown. Biochemical characterisation of the overexpressed protein, including metal analysis indicate an incomplete iron incorporation (~1.4 iron per protein by ICP-AES). This was corroborated by UV-visible and EPR spectroscopies, in which it was demonstrated the single contribution of centre I.

Supplementation with different metals was attempted in order to evaluate *Kc* SOR's ability to incorporate other metals than iron. Incorporation of cobalt was verified by UV-visible and EPR spectroscopies and a content of ~0.4 cobalt per protein was determined.

In order to deconvolute the spectral features of the hypothetically cobalt-bound centre II, a site-directed mutant of a canonical 1Fe-SOR from *Archaeoglobus fulgidus*, H46S, which mimics the non-canonical centre II of *Kc* SOR, was produced and expressed in the presence of cobalt or iron. This protein was able to bind cobalt but not iron, as was verified by ICP-AES, presenting a value of ~0.91 cobalt atoms per protein. The UV-Vis and EPR spectra features of this protein corroborates cobalt incorporation. The crystallographic structure determined for this mutant is almost superimposable to the one from the wild type, apart from the histidine that was substituted by a serine. The density arising from the presence of the cobalt ions was also verified.

A site directed mutant of the *Kc* SOR, S70H, was also produced in order to convert the catalytic centre into a canonical one and to evaluate its ability to bind iron. UV-visible and EPR spectroscopies demonstrated similar features to the wild-type protein. Together with the results of ~0.27 iron per protein obtained by ICP-AES, this indicates, once again, that no metal incorporation occurred in centre II.

A native gel electrophoresis was used to evaluate a possible superoxide dismutase activity of *Kc* SOR, *Kc* S70H and *Af* H46S. The results showed that no SOD activity was detected for the *Kc* SOR supplemented with iron, *Kc* SOR supplemented with iron and cobalt or *Kc* S70H supplemented with iron. In the case of the *Af* mutant H46S, supplemented with cobalt, the data was inconclusive.

Keywords: Superoxide Reductase, *Korarchaeum cryptofilum*, SOR, 2Fe-SOR, neelaredoxin centre, non-canonical centre II.

IV. Resumo

As redutases do superóxido (SOR) são enzimas que catalisam a redução do superóxido a peróxido de hidrogénio. Estes enzimas podem possuir um (1Fe-SOR) ou dois (2Fe-SOR) átomos de ferro não-hémico. Nos enzimas 2Fe-SOR, os átomos de ferro integram dois centros distintos: centro desulforedoxina (centro I) e neelaredoxina (centro II, catalítico). No centro II o átomo de ferro é coordenado por quatro histidinas equatoriais e uma cisteína axial. No centro I, semelhante à desulforedoxina de *D. gigas*, o ferro é coordenado pelos átomos de enxofre provenientes das quatro cisteínas ligantes do motivo de ligação, $CX_2CX_{15}CC$. As características espectroscópicas destes enzimas dependem da incorporação de átomos de ferro nos centros. O centro desulforedoxina oxidado exibe bandas de absorção a 307 e 503 nm, com um ombro a 560 nm, enquanto que, o centro neelaredoxina apresenta bandas de absorção a ~560 nm, ou ~660 nm, na presença de um glutamato ligado ao centro, conferindo a cor azul aos enzimas 1Fe-SOR.

Da análise de sequência de aminoácidos, o enzima de *Korarchaeum cryptofilum* (*Kc* SOR) é previsto ser uma SOR com dois centros de ferro (centros I e II), sendo que uma das histidinas ligantes do centro II está substituída por uma serina. Adicionalmente, o enzima *Kc* SOR possui um domínio extra na região do C-terminal, cuja função é ainda desconhecida. Este trabalho teve como foco principal a caracterização deste enzima, nomeadamente no papel que o seu centro catalítico não-canónico e domínio extra têm na sua actividade enzimática.

Foram realizados testes de expressão para definir quais as melhores condições de expressão deste enzima, seguindo-se produção proteica em grande escala, com a adição de suplementos de ferro e posteriores etapas de purificação da proteína em estudo. No entanto, a caracterização bioquímica desta proteína revelou uma incorporação incompleta de ferro no centro II, sendo que cada proteína possuía ~1.40 átomos de ferro, como determinado por ICP-AES, em vez do esperado de uma 2Fe-SOR, ou seja, 2 ferro por proteína. Este resultado é corroborado por análise espectroscópica de: UV-visível, que demonstra características espetrais apenas do centro desulferoxina, mesmo com adição de um oxidante forte (peróxido de hidrogénio), a contribuição do centro II não foi observada; e de Ressonância Paramagnética Eletrónica (RPE), que comparando com a literatura, mostra apenas características da contribuição do centro I. A ausência do átomo de ferro ou a presença de um metal diferente no centro II não-canónico, são duas justificações para estes resultados.

As SORs têm a capacidade de incorporar diferentes metais para além de ferro, nomeadamente zinco, que por sua vez, não contribuiria o espectro UV-Visível, no entanto, a quantificação efectuada pelo ICP-AES, ~0.05 átomos de zinco por molécula de proteína, permite concluir a ausência deste metal no centro neelaredoxina. Este resultado conduz à hipótese da ausência de metal no centro catalítico. Como tal, para analisar a capacidade deste enzima de incorporar átomos de outros metais, a expressão desta proteína foi repetida com a adição de diferentes suplementos metálicos, como zinco, níquel, cobre e cobalto. Os crescimentos com cobre e zinco não foram bem-sucedidos, verificado por análise por gel SDS-PAGE e espectros de UV-Visível. O crescimento com níquel foi bem-sucedido, mas as análises com os mesmos métodos mostraram uma expressão proteica muito reduzida. A expressão da *Kc* SOR com os suplementos ferro e cobalto foi bem-sucedida. Resultados da análise por UV-Visível quando comparados com a literatura, mostraram características concordantes com incorporação de átomos de cobalto. Contudo, comparativamente com a literatura disponível não foi possível concluir o centro onde ocorreu a incorporação dos átomos de cobalto.

Para determinar os elementos espectrais promovidos pela presença de cobalto no centro II, foi produzido um mutante de uma 1Fe-SOR canónica, H46S de *Archaeoglobus fulgidus* que, ao substituir uma histidina por uma serina, gera um centro II não-canónico semelhante ao verificado no *Kc* SOR. Este mutante foi expresso com suplementação de ferro ou cobalto. Este mutante foi capaz de incorporar cobalto no centro II, mas incapaz de ligar ferro. O tipo selvagem por outro lado, foi capaz de incorporar átomos de ferro, mas incapaz de incorporar cobalto. A incorporação de cobalto no mutante, foi verificada por determinação de metais através de ICP-AES: ~0.91 átomos de cobalto por proteína. As características espectrais observadas por UV-visível e RPE também suportam a incorporação de cobalto. Comparação entre as características espectroscópicas da *Kc* SOR suplementada com ferro e cobalto e o mutante *Af* H46S suplementado com cobalto, apontam pequenas diferenças entre elas, que juntamente com os dados da literatura da rubredoxina e desulforedoxina com incorporação de átomos de cobalto, indicam que para a *Kc* SOR com suplementação de ferro e cobalto, a incorporação de átomos de cobalto ocorra apenas no centro I.

Para verificar se existiria influência do domínio extra na incorporação de metais no centro II, foi expresso o mutante *Kc* SOR S70H com suplemento de ferro, em que o centro II não-canónico foi convertido à forma canónica, com as quatro histidinas equatoriais e a cisteína axial. Os dados de espectroscopia de UV-visível e RPE são semelhantes aos obtidos para o tipo selvagem da *Kc* SOR também suplementado com ferro. Em conjunto com os resultados obtidos por ICP-AES, ~0.28 átomos de ferro por proteína, é possível concluir que não ocorreu incorporação de ferro no centro II canónico. Estes resultados levam à hipótese de uma influência do domínio extra na capacidade de incorporação de metal no centro II. Para confirmar esta hipótese, foi feita uma tentativa para esclarecer a estrutura da *Kc* SOR por cristalografia de raios-X. Infelizmente, cristais obtidos deste enzima não possuíam qualidade de difração suficiente para a determinação da sua estrutura. Foi, no entanto, possível determinar a estrutura da *Af* mutante, H46S, suplementada com cobalto. A estrutura tridimensional determinada, confirmou a incorporação de átomos de cobalto no centro neelaredoxina, com a coordenação de três histidinas e de uma cisteína axial, sendo quase sobreponível com a do tipo selvagem, com a excepção do resíduo mutado.

Sendo um novo centro catalítico nunca visto numa SOR, a capacidade de dismutação de superóxido das proteínas em estudo foi avaliada por eletroforese em gel PAGE-nativo seguido de coloração com nitroazul de tetrazólio. Os resultados demonstram a ausência de actividade de dismutação para o tipo selvagem da *Kc* SOR suplementado com ferro e com ferro e cobalto, e para o mutante *Kc* S70H suplementado com ferro, sendo, porém, inconclusivos para o mutante *Af* SOR H46S suplementada com cobalto. Juntamente com os dados que confirmam a incorporação bem-sucedida de cobalto na *Af* SOR H46S, pode especular-se que este enzima pode requerer um substrato diferente.

Neste trabalho foi possível concluir, que a *Kc* SOR parece ser incapaz de incorporar ferro, o cofator característico de redutases do superóxido, tanto tipo selvagem como no mutante S70H. Os resultados obtidos parecem indicar a hipótese de que o domínio extra na região do C-terminal pode ter implicações na incorporação de metais no centro catalítico. Além do ferro, este enzima foi incapaz de incorporar outros metais, podendo afetar a capacidade de usar superóxido como substrato para a actividade enzimática. O mutante *Af* H46S, com átomos de cobalto incorporados no centro II, foi incapaz de usar superóxido como substrato, este sugere que a incorporação de cobalto impede a actividade de dismutação do superóxido e, consequentemente, a possibilidade deste enzima com este centro não-canónico usar um substrato diferente.

Palavras-chave: redutases do superóxido, 2Fe-SOR, *Korarchaeum cryptofilum*, centro neelaredoxina, centro II não-canónico.

V. Index

VI. Figures

VII. Tables

1. Introduction

1.1. Oxidative stress and response enzymes

When life first appeared on Earth, around 3.5 billion years ago, the atmospheric levels of oxygen were very low. However, approximately 2.2 billion years ago, a rise in oxygen occurred due to the photosynthetic metabolism of cyanobacteria,[1] which became known as the Great Oxidation Event. In this new oxidative environment, the existing metabolic pathways were reshaped, resulting in others not yet observed[2], leading to the appearance of organisms adapted to an aerobic lifestyle.

Molecular oxygen is a powerful four-electron oxidizing agent and its complete reduction with four electrons originates water (Eq. 1.1). However, it can also be reduced in four sequential one-electron steps (Eq. 1.2-5), which generates Reactive Oxygen Species (ROS).

$$O_2 + 4H^+ + 4e^- \rightarrow 2H_2O \qquad 1.1)$$

$$O_2 + e^- \rightleftarrows O_2^{\bullet -} \qquad 1.2)$$

$$O_2^{\bullet -} + 2H^+ + e^- \rightarrow H_2O_2 \qquad 1.3)$$

$$H_2O_2 + H^+ + e^- \rightarrow H_2O + OH^{\bullet} \qquad 1.4)$$

$$OH^{\bullet} + H^+ + e^- \rightarrow H_2O \qquad 1.5)$$

ROS are highly reactive molecules that can be divided in free radicals, like the superoxide anion ($O2^{\bullet -}$), hydroxyl radicals ($OH^{\bullet}$), peroxyl ($ROO^{\bullet}$), alkoxyl ($RO^{\bullet}$) and hydroperoxyl ($HO_2^{\bullet}$), and non-radical intermediates such as hydrogen peroxide (H_2O_2), ozone (O_3) and singlet oxygen ($^1O_2$).

Physiologically, ROS can be produced by several processes. For instance, in innate immune responses, phagocytes produce ROS during the respiratory burst. In this mechanism, the enzyme NADPH-oxidase generates the superoxide radical that can be converted to hydrogen peroxide[3] by superoxide dismutase.[4] ROS can also be produced during oxidative phosphorylation (the respiratory complexes I and III produce superoxide), and in inflammatory and tissue-injury responses and can act as signalling molecules and inflammation mediators.[5] Moreover, ROS can also be produced exogenously as a result of exposure to factors such as pollutants, drugs or radiation.[6]

ROS are very deleterious due to their ability to interfere with several cell targets with key biological functions like proteins, lipids and DNA. Specifically, ROS can cause protein cleavage, cross-linkage and loss of structural and/or catalytic function,[7] lipid oxidation[8] and DNA damage[9] through modification of nitrogenous bases. Protein degradation is an issue of particular concern since it can go unnoticed by the cell's protein degradation systems, leading to the accumulation of abnormal proteins. Nonetheless, it is noteworthy to mention that besides their harmful effects, ROS can also be beneficial. For example, ROS have been found to be required for the genesis of otoconia, small calcium carbonate crystals present in the inner ears of mammals that are essential for the perception of gravity and balance.[10] This further highlights the importance of understanding enzymes involved in the control of ROS levels.

In particular, so far, only two enzymes capable of regulating the levels of the superoxide radical are known (Fig. 1): superoxide dismutase (SOD) and superoxide reductase (SOR). The superoxide radical may act as a toxic species or as a signalling agent. SOD and SOR are redox-active metalloenzymes that evolved independently from one another. SOD enzymes, of which five distinct types have been described to date, contain Fe, Mn, Ni, Cu, or Cu and Zn ions in their catalytic site,[11] and dismutate superoxide into hydrogen peroxide and oxygen (Eq. 1.6).

$$2O_2^{\bullet-} + 2H^+ \xrightarrow{SOD} O_2 + H_2O_2 \qquad 1.6)$$

On the other hand, SOR enzymes contain only iron at their catalytic centre and catalyse the one-electron reduction of $O_2^{\bullet-}$ to hydrogen peroxide (Eq. 1.7).[12] These enzymes will be the main focus of this thesis.

$$O_2^{\bullet-} + 2H^+ + SOR_{red}{}^{x} \rightarrow SOR_{ox}{}^{X+1} + H_2O_2 \qquad 1.7)$$

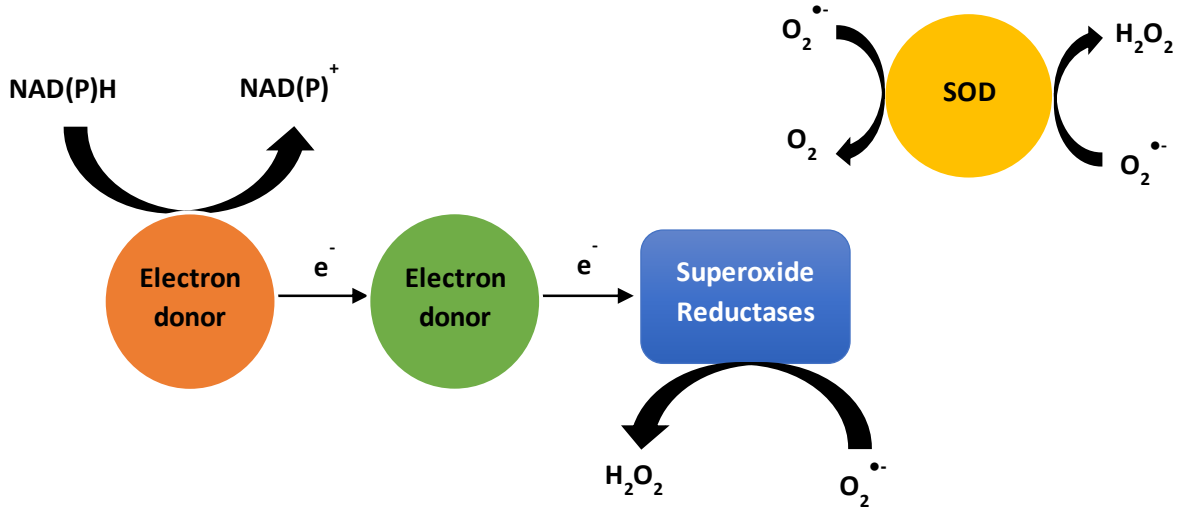

Figure 1 - Schematic representation of superoxide reductase and dismutase reactions. From the pool of NAD(P)H electrons are delivered to the electron donors, and subsequently transferred through a NAD(P)H oxidoreductase (e.g., NADH rubredoxin oxidoreductase) to another electron transfer protein (e.g., rubredoxin); this last redox protein then donates electrons to SORs for reduction of the respective substrate. SODs on the other hand, are stand-alone enzymes.

1.2. Superoxide reductase proteins

The first SOR was discovered in anaerobic sulfate reducing bacteria of the *Desulfovibrio* (D.) genus. The SOR desulfoferrodoxin (Dfx), which was isolated from *D. vulgaris* Hildenborough and *D. desulfovibricans* ATCC 27774,[13] was named this way for the iron centre present – centre I – similar to the desulforedoxin (Dx), a protein related with rubredoxins with a FeCys4 site[14]; this centre is also called, desulforedoxin centre. The Dfx has another iron centre – catalytic centre II – which has a high homology to another iron containing protein, neelaredoxin (Nlr), isolated first from *D. gigas*. In the neelaredoxin centre, the iron ion is coordinated by four equatorial histidines and one axial cysteine, and its name derives from its blue colour in the oxidised (ferric) state.

Complete genome sequences analysis from anaerobic organisms, such as *Methanococcus janmaschii*,[15] *Archaeoglobus fulgidus*,[16] *Pyrococcus* horikoshii[17] and *Thermotoga maritima*,[18] did not show presence of SOD and catalase genes when compared with aerobic organisms. Further investigation suggested the presence of an enzyme involved in oxygen metabolism. Their function as superoxide reductase was established by Jenney and co-workers using SOR from *Pyrococcus* (*P.*) *furious*.[19] Purification of cell-free extracts with SOD activity from the anaerobic hyperthermophile *P. furious*,[19] led to a "putative SOD", with a sequence similar with neelaredoxin from *D. gigas*. In the standard SOD assay, both native and recombinant forms of the "putative SOD" exhibited high activity, comparable to the bovine SOD in the same conditions.[13] There was, however, a difference in the proprieties of the two enzymes. In both cases the rate of cytochrome c reduction decreased with increasing amounts of enzyme, an excess of the protein purified from *P. furious* caused a reoxidation of the reduced cytochrome c, whereas in the case of bovine SOD this effect was not observed.[13] The use of the xanthine/xanthine oxidase system led to the conclusion that the *P. furious* protein appears to function as a superoxide reductase. Later on, the desulfoferrodoxin from *D. baarsii* was also proposed to be a superoxide reductase,[20] as well as the SOR from *Treponema pallidum*.[21]

The classification of SORs is based on amino acid sequence analysis. There are two main groups of SORs, the 1Fe-SOR with one iron in the catalytic centre II (neelaredoxin centre), and 2Fe-SOR with the same catalytic centre II and an additional iron in the centre I (desulforedoxin centre). The catalytic centre of the 1Fe-SORs shares sequence homology with the catalytic centre II of 2Fe-SORs and the N-terminal domain of 2Fe-SORs is homologous to desulforedoxins. Other classes have been proposed based on the extra domains found by amino acid sequence analysis. Bioinformatic analysis of genomic sequences identified 7 classes of SORs[20] that, with the exception of methanoferrodoxins, contain one or two iron centres (the catalytic centre and the Dx-like centre). [22]

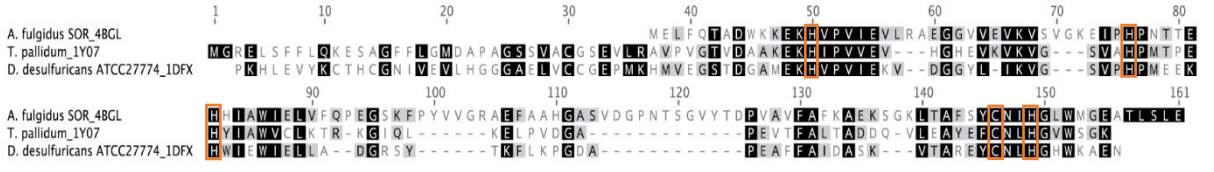

Figure 2 - Amino acid sequence alignment of canonical superoxide reductases. *A. fulgidus* SOR (*Af* SOR), a 1Fe-SOR protein with an iron on the neelaredoxin centre (centre II); *T. pallidum*_1Y07 is a 1Fe-SOR protein with an iron in the neelaredoxin centre, similar with the *Af* SOR, except for the first 36 aa which are similar with the *D. desulfuricans* Dfx. *D. desulfuricans*, Dfx is a 2Fe-SOR canonical protein with iron in both neelaredoxin centre and the desulforedoxin centre (centre I). Neelaredoxin centre histidine and cysteine ligands are highlighted.

1.2.1. Superoxide Reductase Structure

Over the years, different crystallographic structures were obtained for SORs (Table 1). The 1Fe-SORs are homotetramers, with four monomers organised in pairs of antiparallel subunits (Fig. 3 - A), forming a cube with the active centres diagonally oriented at opposite positions. The neelaredoxin centre is localized in a domain with a 3 + 4 stranded β-barrel in an immunoglobulin-like fold. The iron coordination in the catalytic centre is composed by four equatorial histidine imidazole nitrogen's (three Nε and one Nδ) and by a sulphur from a fifth axial cysteine. (Fig. 3 - A) The metal ligands are in the loops connecting the β strands. This catalytic centre also appears on 2Fe-SOR proteins, which are homodimers (Fig. 3 - B), where each subunit is composed by two structural domains. The neelaredoxin centre resides in one of the domains similar to that of 1Fe-SORs. The second domain at the N-terminal, resembles desulforedoxins and contain a slightly distorted tetrahedral site, similar to *D. gigas* desulforedoxin (Dx), where the iron is coordinated by the sulphur atoms of four cysteines, with the binding motif $CX_2CX_{15}CC$ (Fig 3 - B). It has been shown that the [FeCys4] centre I from the 2Fe-SORs does not participate in the oxidative part of the catalytic cycle, in the reduction of superoxide to hydrogen peroxide.[23]

Table 1 - Available crystallographic structures of SORs. *These data contain both the oxidised, glutamate-bound, and the reduced forms. Adapted from Pinto, Ana *et al* (2010)

SOR type	Domain	Organism	PDB	Resolution (Å)	Wild type/mutants	References
1Fe-SOR						
	Archaea	*P. horikoshii*	2HVB	2.5	WT	Structural genomics
	Archaea	*P. furiosus*	1DQI	1.7	WT	[24]
			1DO6	2	WT	[24]
			1DQK	2	WT	[24]
	Bacteria	*T. maritima*	2AMU	2	WT	Structural genomics
	Bacteria	*T. pallidum*	1Y07	1.55	WT	[25]
		A. fulgidus	4BGL	1.90	WT	[26]
			4BFF	2.0	WT	[27]
2Fe-SOR						
	Bacteria	*D. desulfuricans* ATCC2774	1DFX	1.8	WT	[28]
	Bacteria	*D. baarsii*	2JI3	1.9	E114A	[29]
			2JI2	1.9	E114A	[29]
			2JI1	1.9	WT	[29]
			1VZI	1.7	E47A	[30]

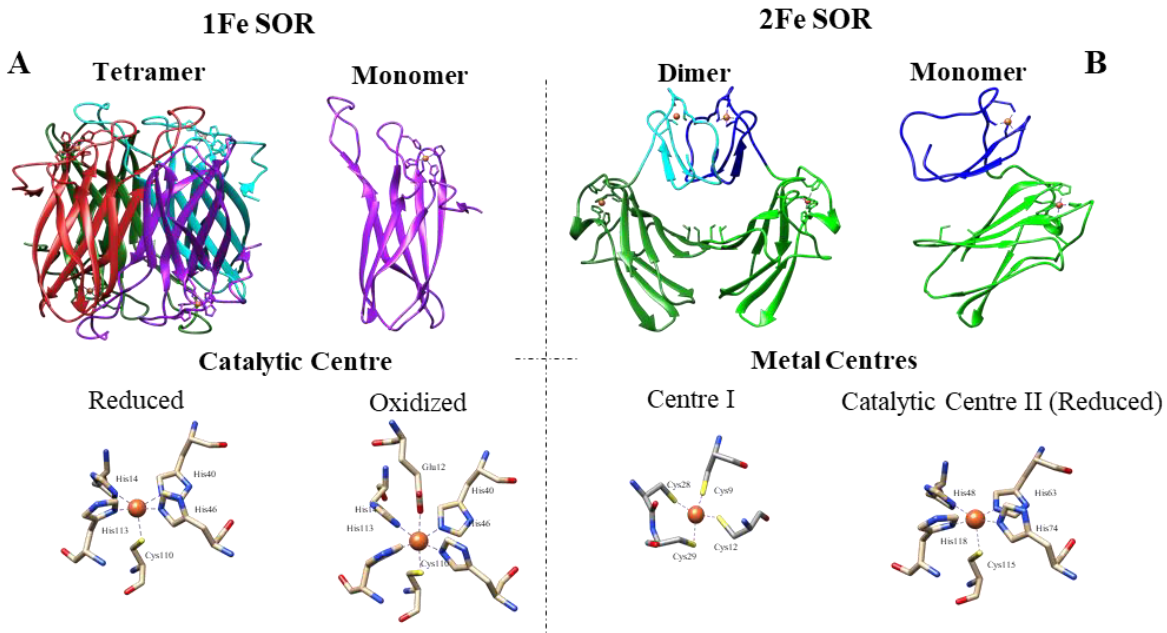

Figure 3 - Structure of 1Fe and 2Fe-SORs. (A) Crystallographic structure of a 1Fe SOR (*A. fulgidus*, PDB code 4BFF) in its tetrameric and monomeric forms; each subunit is represented with a different colour. The structure of the catalytic centre in the oxidised and reduced states is shown. (B) Crystallographic structure of a 2Fe SOR (*D. desulfuricans*, PDB code 1DFX) in its dimeric and monomeric forms. Each subunit is represented with two colours according to the two domains: Dx (blue) and Nlr (green) domains. The structure of the metal centres is shown: Centre I, a desulforedoxin-like one with four cysteines coordinating the iron, and Centre II in the reduced state. The iron is represented by red spheres. Figure prepared with Chimera.

The neelaredoxin centre has two forms, the reduced (active) form and the oxidised form. In the oxidised form, the catalytic centre has, in most cases, an octahedral coordination, holding the iron ion. This coordination is fulfilled by a glutamate carboxylate in the opposite position to the axial cysteine. In the reduced form, the catalytic site is coordinated by four histidines and the axial cysteine, forming a square pyramidal geometry. The cysteine ligand was shown to be essential for SOR activity.[31] During the transition from the oxidised to reduced state, the catalytic site undergoes a structural change at the N-terminal region, which contains lysine and glutamate residues that have, been proposed to play a role in the overall catalytic mechanism. The glutamate ligand moves further away from the catalytic centre, and the lysine residue comes closer, however it does not become a coordinating ligand since its distance from the iron ion ranges from 3.6-8.9 Å. On account of X-ray crystallography, the reduced and oxidised forms can be seen to adopt two different conformations: open and closed, respectively. The open conformation of the reduced form, allows a charged lysine residue to attract the superoxide anion substrate to the free axial position, and helps stabilize the catalytic intermediates.[29,32,33]

While the lysine and glutamate residues are important for a large population of SORs, there are a few cases where they are absent. Nonetheless, studies showed that the kinetic rate constants in the absence of these residues are close to those of the canonical enzymes.[34]

1.2.2. Spectroscopic properties of the Iron centres

The properties of the catalytic centres of the 1Fe and 2Fe SORs have been thoroughly analysed by spectroscopic methods, primarily UV-visible spectroscopy but also resonance Raman, EPR, Mössbauer, and FT-infrared. This allowed some understanding of the electronic properties of the sites and their reactivity with the substrate, the $O_2^{\bullet-}$ anion, and other small ligands. Namely, electronic absorption spectroscopy allowed the easy distinction of both iron sites. The FeCys4 site, has the characteristic features of an oxidised desulforedoxin centre, exhibiting bands at 307 and 503 nm and a broad shoulder at 560 nm, due to cysteine sulphur to metal charge transfer transitions.[35] SORs centre II has a broad absorption band at ~560 (in glutamate-lacking enzymes) or ~660nm, which gives rise to the blue colour of 1Fe-SORs or the grey colour of the fully oxidised form of 2Fe-SORs (resulting from the mixture of blue with the pink colour of the Dx site). In the fully reduced state both types of SORs are colourless, while the half-reduced (centre I oxidised, centre II reduced) 2Fe-SORs are pink.

There are studies showing a pH dependency of the catalytic site. In the oxidised state, for enzymes with glutamate ligand, a small shift in the spectra can be seen, from 660 to approximately 590 nm with a pKa of ~9.5. In the reductase reaction, the consumption of two protons can be observed at physiological pH, when the superoxide anion is deprotonated (pKa ~4.8), and the product is fully protonated, highlighting the relevance of pH control for the catalytic mechanism.

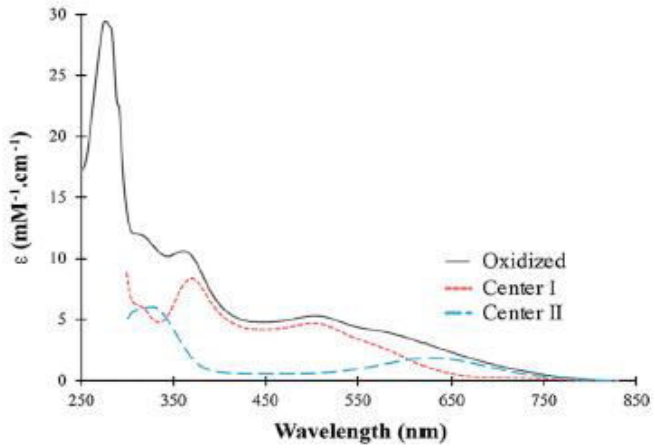

Figure 4 - UV–visible spectra of a 2Fe-SOR. Grey solid line represents the spectrum of the fully oxidised form; Pink dashed line represents the spectrum of the oxidised Centre I and the Blue dashed line the spectrum of the oxidised Centre II. From M. C. Martins et al 2019

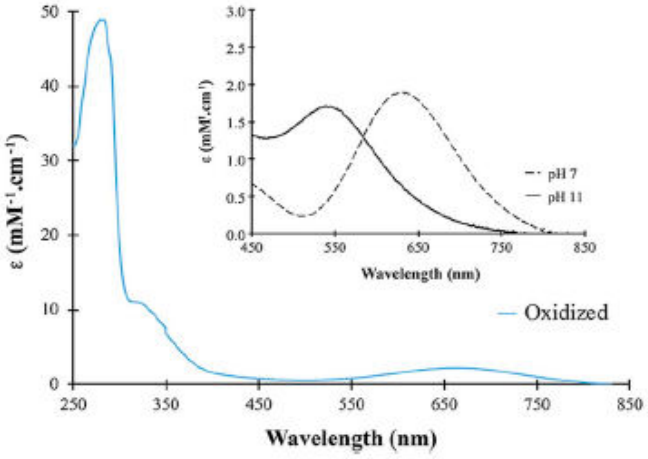

Figure 5 – UV-visible spectrum at neutral pH of a 1Fe-SOR in the oxidised state. The inset represents the pH dependent spectra of the same protein at pH 7 (dashed line) and at pH 11 (solid line). From M. C. Martins et al

Resonance Raman spectroscopy[36] detected a vibrational band ate 466-471 cm^{-1}, showing that a high-spin Fe-hydroxide stretching mode is formed, that appears with increasing pH and disappears at acidic values. The glutamate ligand is replaced by a hydroxide anion[37]:

$$His_4CysFe\text{-}Glu_P + OH^- \rightarrow His_4CysFe\text{-}OH + Glu_P^- \qquad 1.8)$$

This has been observed by Fourier-transform infrared spectroscopy[38] and by EPR spectroscopy.[39] In SORs without the glutamate ligand, whether wild type proteins or mutants, a pH-dependent equilibrium is also observed, with a lower pKa, corresponding to a hydroxide-bound iron form. In this case a true protonic equilibrium causes the pH dependency:

$$His_4CysFe\text{-}(H_2O) \rightarrow His_4CysFe\text{-}OH + H^+$$
$$\text{or}$$
$$His_4CysFe + OH^- \rightarrow His_4CysFe\text{-}OH \qquad 1.9)$$

These pH-dependent processes are important to understand the reactivity of SOR proteins with superoxide, and were shown to affect (*i.e.,* decrease), the reduction potentials of centre II from the *D. baarsii* 2Fe-SOR.[39]

More specifically, although the redox potentials are pH-dependent, in this case they are constant in the range 5.5 - 9, which can also be said for *I. hospitalis* 1Fe SOR. With the use of EPR and redox titrations, the neelaredoxin centre reduction potentials were observed to range from +190 mV to +360 mV at pH ~7, depending on the enzyme, and the potential of the desulforedoxin centre ranges from +4mV to 60 mV, at the same neutral pH, akin to the isolated *D. gigas* desulforedoxin.[14] In SOR mutants of the glutamate ligand, the potentials fluctuate more with the pH, with a pKa_{ox} of 6.5 and a ~60 mV decrease per pH unit. At higher pH values the reduction potential decreases and at acidic pH the potential increases, and this phenomenon is believed to be caused by a H_2O molecule bound in the glutamate "open space".

1.2.3. Catalytic cycle

To understand how SORs are able of reducing O_2^- it is necessary to study the catalytic mechanism behind it. Techniques like pulse radiolysis,[26,40–43] stopped flow, UV-visible spectroscopy, EPR and Raman and Mössbauer,[36,41] were essential to the identification of the catalytic intermediates. In the beginning of the catalytic cycle (Fig 6), the active enzyme is in the ferrous pentacoordinate state and it does not have absorption bands in the visible region, thus being colourless.

The first intermediate (I1) of the SOR catalytic mechanism appears to be common among all SORs known so far and has a characteristic absorbance maximum at *ca.* 620 nm, suggesting that the iron is already in the ferric state Fe (III). However, for this first intermediate two possible formulations were proposed: a ferric end-on hydroperoxide form (Fe (III)-OOH)[44,45] (I1) or a short-lived ferrous end-on superoxide species (Fe (II)-$O2^-$),[38] (I1*) with the first being generally more accepted.

In the ferric-hydroperoxide species (I1), the peroxide ion must be protonated for the hydrogen peroxide to be released. For some SORs, I1 decays into another intermediate, I2. This second intermediate has similar optical properties to the basic form of ferric SORs, and to the Fe (III)-hydroxide form of *A. fulgidus* SOR, specifically an absorption band at *ca*. 590 nm. In some enzymes

like *Af* SOR, I2 further decays to an oxidised state, while in others it can be the final state of the oxidative half of the cycle. There are also SORs for which I2 is not detected and I1 directly decays to the final species of the cycle, which is identical to the oxidised state of I2. However, it is still under debate whether in these cases I2 really does not exist or if it is so short-lived that it cannot be detected. For example, two intermediaries can be detected for the 2Fe-SOR of *D. baarsii* and the 1Fe-SOR of *T. pallidum*, but only I1 is detected for *D. vulgaris* SOR.

The reductive path of the catalytic cycle needs electrons to occur, more specifically, it needs physiological electron donors. For most SORs the electron donors are the rubredoxins (small electron transfer proteins with an iron ion coordinated by four cysteines sulfurs).[46] Rubredoxins are very efficient with elevated second-rate constants and are capable of reducing both centre I and centre II, and in turn they are reduced by NAD(P)H oxidoreductases.[25,47,48] It is possible to hypothesize the existence of others physiological electron donors, since many organisms with SORs encoding genes, do not have rubredoxin or desulforedoxins coding genes.

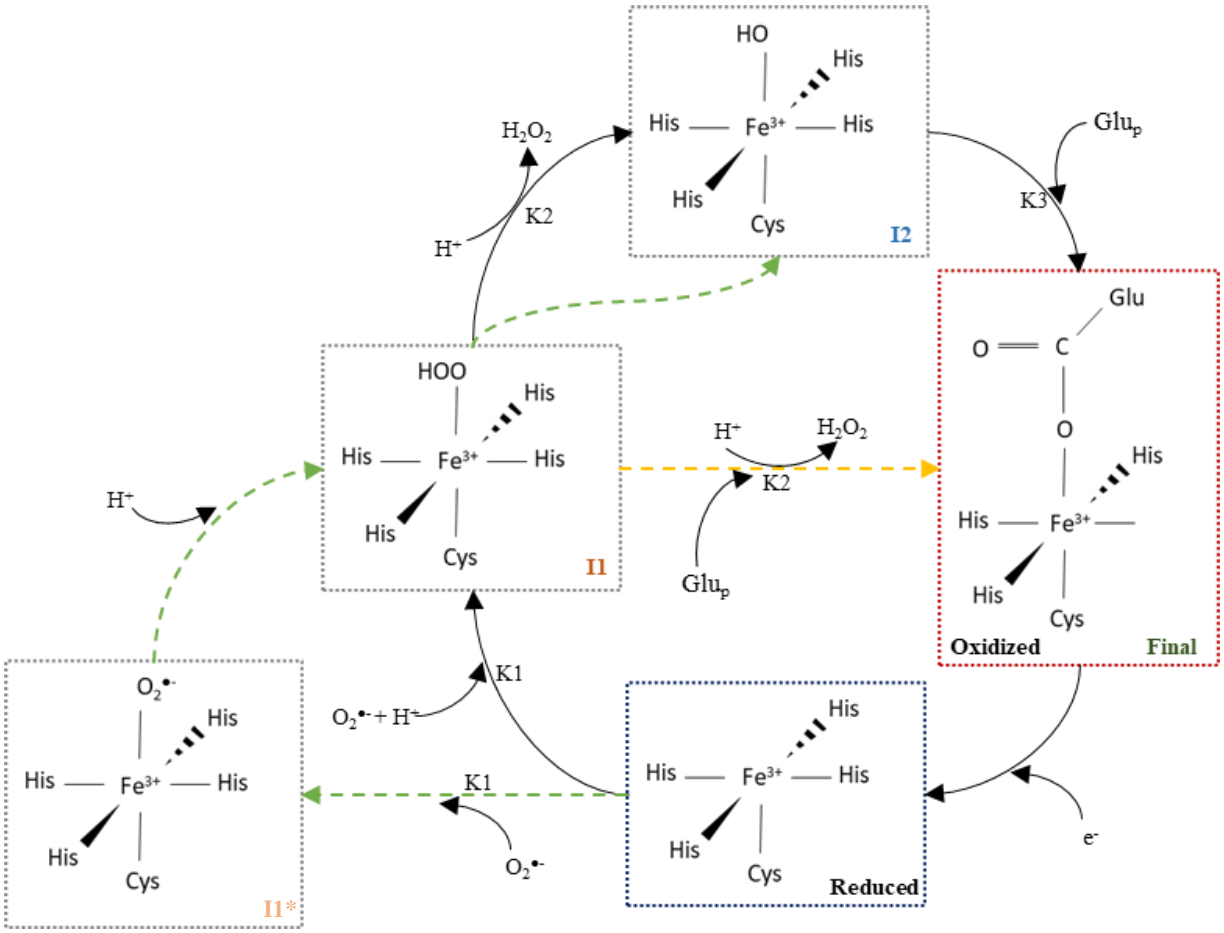

Figure 6 - Catalytic mechanism of SORs. Schematics of the two possible structures for I1 and the two mechanisms involving one or two macroscopically observed intermediates (I2). Proposed route from I1* to I2 is represented in green dashed line, and the alternative macroscopically route from I1 to the final oxidised state is represented in yellow dashed line.

1.3. Non-canonical Superoxide reductase proteins

Canonical superoxide reductases are protein that exhibit the general common properties of this class of enzymes. Non-canonical SORs are designated as such, on the account of natural mutations or extra domains present in their structure. The *Korarchaeum cryptofilum* SOR has a putative non-canonical neelaredoxin centre, where one of the histidine ligands is substituted by one serine, and it also has an extra domain in the C-terminal.

In this work, other SORs were used, namely a mutant of the *Kc* SOR, that has a histidine instead of a serine in the catalytic centre II. Due to this residue replacement, this mutant should display a canonical catalytic centre, distinguishable from other canonical SORs by the presence of the unknow extra domain. Henceforward this mutant will be referred to as *Kc* S70H.

As both SORs described above are non-canonical, a known canonical SOR was needed as a positive control. After preliminary observations of the *Kc* SOR it was defined that the catalytic centre II (neelaredoxin centre) and the extra domain were going to be the main focus of this investigation, since nothing unusual occurred with the non-catalytic centre I (Dfx). This led to the choice of the *Archaeoglobus fulgidus* SOR (1Fe-SOR), hereafter referred to as *Af* SOR. Besides the wild type *Af* SOR, the mutant protein *Af* H46S was also used. Instead of a histidine in the position 46, this mutant has a serine, meaning that it, has the same non-canonical catalytic centre II as the *Kc* SOR, although it does not have the extra domain that may cause conformational constraints.

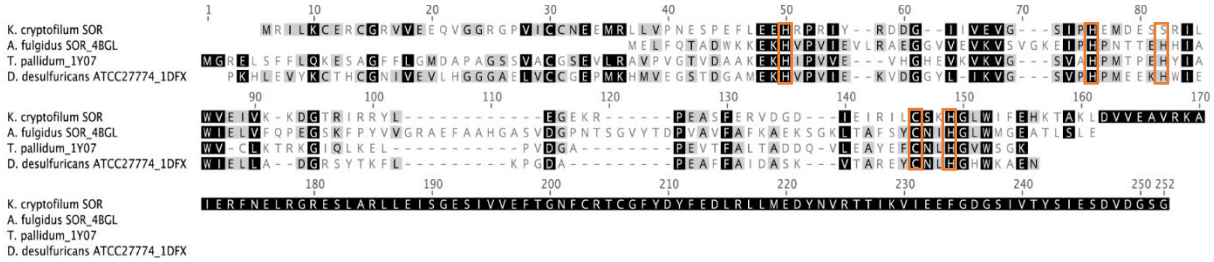

Figure 7 – Amino acid sequence alignment of the non-canonical *K. cryptofilum* SOR with canonical 1Fe- and 2Fe-SORs. *K. cryptofilum*, Fe-SOR protein with both catalytic centres, the main difference between the *Kc* SOR and the canonical SOR is the extra domain (aa 162 – 252) and the *A. fulgidus* mutant H82S, highlighted.

1.3.1. *Candidatus Korarchaeum cryptofilum*

Korarchaeum constitutes a little characterised phylum from the *Archaeal* domain, and it is a division associated with hydrothermal environments. These organisms have a subunit (SSU) rRNA gene sequence that can be traced back to some ancient phylogenetic lineages, which may have diverged early from the major archaeal phyla *Crenarchaeota* and *Euryarchaeota*. The *Korarchaeota* have a large number of unclassified *Archaea* and there is evidence of the presence of these organims in several isolated thermal environments, as much as terrestrial as marine.[49–51]

To further study the division *Korarchaeota*, investigators from the Elkins group in 2008, collected several SSU rDNA sequences samples from thermal geographical locations, like the Obsidian Pool at Yellowstone National Park (YNP) in Wyoming. An ultrathin filament with a diameter between 0.16 and 0.18 µm and variable length was identified. With the help of whole-genome shotgun (WGS) sequencing, the whole genome was obtained. The identified organism was designated *Candidatus Korarchaeum cryptofilum*.[52]

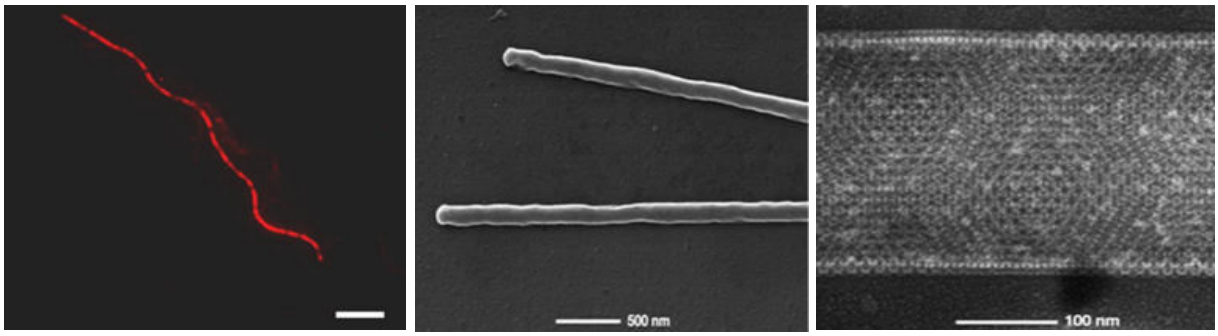

Figure 8 - *Candidatus Korarchaeum cryptofilum* - From left to right. Fluorescence in situ hybridization analysis of *Candidatus Korarchaeum cryptofilum* Ca. *K. cryptofilum* with Korarchaeotaspecific Cy3-labeled oligonucleotide probes KR515R/KR565R (Scale bar, 5 µm.); Scanning electron micrograph of purified cells; Transmission electron micrograph after negative staining with uranyl acetate displaying the paracrystalline S layer. From Elkins *et al* (2008)

This organism is suggested to be symbiotic or an efficient scavenger of essential co-factors, vitamins and purines, since it cannot synthesize them. It is capable of obtaining energy through fermentation and is an efficient peptide degrader.

Through data base sequences analyses a new type of 2Fe-SOR protein was discovered, with an unfamiliar extra domain in the C-terminal as well as a mutation in the catalytic centre II; one of the histidines ligand is substituted by one serine, raising the question of whether this protein is able to bind iron at the centre II. This SOR was the main focus of this work and through this work this protein is going to be referred as *Kc* SOR.

1.4. Cobalt as a co-factor

Metalloenzymes and metalloproteins are known to use iron, zinc, magnesium, manganese and calcium as co-factors for their functions, among other metals, but several enzymes incorporate cobalt cations.[53] For example, cobalt is a co-factor of vitamin B_{12}, where it is present at the centre of the substituted corrin macrocycle, and it also plays several crucial roles in many biological functions, as in the activation of α-D-mannosidase in the rat liver.[54] Cobalt is a transition metal with two naturally occurring oxidation states, Co^{2+} and Co^{3+}, which display distinct spectral features and can therefore be used as spectroscopic probes for metalloenzymes.[55] Cobalt (II) also stabilizes some transcriptional activators, including the one known as hypoxia-inducible factor (HIF)[56] that regulates erythropoietin production, thus being involved in several adaptive responses to hypoxia.[57]

Cobalt incorporated in catalytic centres is usually bound by glutamate, aspartate and histidine residues[58]. Cobalt is rarely bound by cysteines residues,[59] however, an example is nitrile hydratase of *B. smithii* where the cobalt atom is coordinated by three cysteines and one serine.[60] Cobalt centres can also be binuclear as in the case of prolidase and methionine aminopeptidase of *P. furiosus*.[61,62] In these proteins, an aspartate and glutamate simultaneously coordinate the two cobalt atoms. One cobalt is further bound by a second aspartate residue, while the other is also bound by a histidine and a glutamate. Interestingly, the di-iron DNA-binding protein from starved cells (Dps)[63] and Dps-like peroxide resistance protein (Dpr)[64] were also found to be able to bind cobalt.[65,66] In the first, the cobalt atom is coordinated by an aspartate, a histidine, a glutamate and two water molecules, and the second exhibits a similar coordination sphere but with one less water ligand.

SAD phasing based on Co atoms is a convenient structure-determination strategy for macromolecular crystallography.[67] For instance, the structure of the proteins *M. lini* AvrL567-A[67] and Sentrin-specific protease 1 (SENP1)[68] was resolved after co-crystallisation with cobalt.[67]

2. Aim of this dissertation

The aim of this thesis is to produce and characterise biochemically, spectroscopically and structurally the novel superoxidase reductase from the *Candidatus Korarchaeum cryptofilum*, which is predicted to be a 2Fe-SOR enzyme, with a non-canonical catalytic centre and an extra domain in the C-terminal region. This thesis also aims to understand the effect of the substitution of one of the iron-ligand histidines by a serine on the enzyme's capability to incorporate metal ions as well as its activity. Studies of mutated canonical 1Fe-SORs mimicking this non-canonical catalytic centre will be performed to further understand this natural mutation implications. The role and implication of the unknow extra C-terminal domain will also be targeted with attempts of structure determination by X-ray crystallography.

3. Methods

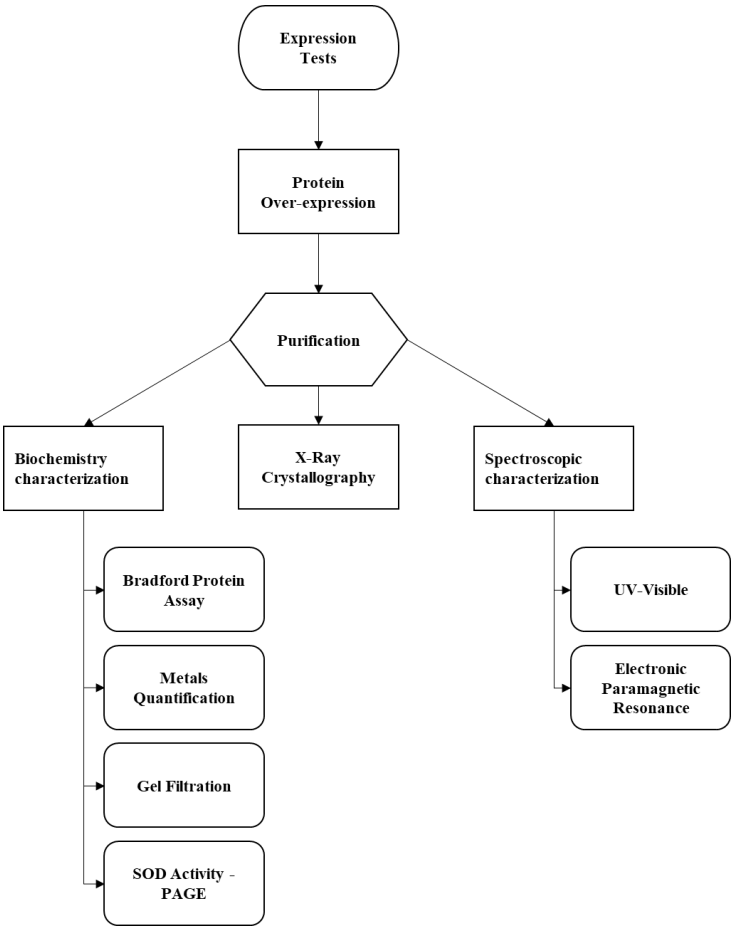

Figure 9 - Methods workflow chart. Proteins of this work went through two different paths after isolated. Biochemical characterisation which involved protein and metal quantification of the purified sample, gel filtration to determine the quaternary structure and NATIVE-PAGE gel to determine the presence of superoxide dismutase activity. Spectroscopic characterisation through UV-Visible, EPR and structural characterisation by X-ray crystallography in order to determine protein's structure and to study metal coordination.

3.1. Transformation

3.1.1. Gene expression

Heterologous expression of the *Korarchaeum cryptofilum* and *Archaeoglobus fulgidus* SORs and site-directed mutants, S70H and H46S, respectively, was performed in *E. coli* BL21 (DE3) cells (Appendix 3). These BL21 strains are ideal for performing protein expression studies that utilize the T7 RNA polymerase promoter to direct high-level expression. Derived from *E. coli*, these expression strains naturally lack the Lon protease, which can degrade recombinant proteins. Transformed cells harbouring the correspondent plasmids were plated into LB-Agar containing 50 mg/mL kanamycin and grown overnight at 37 ºC. A single colony was used to inoculate a pre-inoculum in LB medium. Lysogeny broth (LB) medium, is the most common media used for maintaining and cultivating laboratory recombinant strains of *Escherichia coli.*[69]

Figure 10 – *Korarchaeum cryptofilum* SOR and *Archaeoglobus fulgidus* mutant *H46S* transformation on agar plates, with kanamycin, overnight incubation, 37 ºC. (Left) Bacterial colonies of 100 µL competent cells with DNA plasmid *Af* H46S, (Right) Bacterial colonies of 200 µL competent cells with DNA plasmid *Kc* SOR

3.1.2. Pre-inoculum

In this work, pre-inoculum necessary for protein overexpression, followed the same protocol, varying the volumes used, depending on the size of overexpression intended. A single colony from transformation gene and expression was used to inoculate the pre-inoculum in LB medium containing 50 mg/mL kanamycin and left growing overnight at 37 ºC and 180 rpm.

Figure 11 – *Korarchaeum cryptofilum* SOR pre-inoculum before and after incubation. (Left) Pre-inoculum of *Kc* SOR at time zero, (Right) *Kc* SOR pre-inoculum after overnight incubation at 37ºC, 180 rpm.

3.1.3. Isolation and purification of pDNA

A miniprep kit (NZYSpeedy Miniprep, Nzytech®) was used to isolate plasmid DNA from bacterial cultures. Competent *E. coli* DH5-α cells were used for the transformation step. Single colonies were picked from fresh streaked selective plates and inoculated into LB medium containing kanamycin. The culture was incubated for 14 h at 37 ºC with vigorous shaking. The procedure can be simplified in 5 steps (Appendix 4), that use spins with different time spans, at room temperature, in a table-top microcentrifuge (VWR®). First, cells are harvested and lysed. Afterwards, the extract is loaded into the kit columns and several washing steps are performed before the plasmid DNA is eluted.

3.2. Expression tests

In order to determine the optimal overexpression conditions for *Korarchaeum cryptofilum* SOR, expression tests were conducted by testing the moment of induction (OD of induction) and the amount of inductor, isopropyl β-D-1-thiogalactopyranoside (IPTG). All procedures involving cells growth, were conducted in a sterile environment, being all solutions sterilized before use and open and used next to a flame.

For the expression tests, minimal medium (M9) was used in 8 Erlenmeyer of 200 ml, adding the following supplements: $MgSO_4$ (2 mM), $CaCl_2$ (100 mM), glucose (200 mM), kanamycin (50 µg/mL), iron (10 µM $FeSO_4$), 150 mL of Milli-Q H_2O and 6 mL of pre-inoculum. Gene expression was induced with different concentrations of IPTG (0, 0.1, 0.5 and 1 mM) adding 0.2 mL of 0.1 M iron sulfate at $OD_{0.4}$ and again at OD_1. After inducing, the OD was checked at pre-determined times 2, 4 and 20 hours after IPTG induction.

A sample from each checkpoint was saved and later analysed by SDS-PAGE to observe target protein expression.

3.3. Protein overexpression

3.3.1. *Korarchaeum cryptofilum*

In this work, the protein overexpression protocol was similar for all proteins with the exception of the metal supplements (Table 2). Cells were grown in M9 medium (Appendix 1) supplemented with 50 µg/mL kanamycin and 100 mM $FeCl_2$, (Table 2), at 37 ºC and 180 rpm, until OD_{600nm} 0.3 - 0.5. Protein overexpression was induced with 0.1 mM IPTG and supplemented with $FeCl_2$, $FeCl_2$ and $CoCl_2$, or $FeCl_2$ and $NiCl_2$ (Table 2), for 18 h at room temperature.

3.3.2. *Archaeoglobus fulgidus*

For *Af* SOR wild type and H46S mutant the procedure was adapted from the literature.[26] The cell culture was supplemented with 100 mM of $FeCl_2$ or $CoCl_2$. Protein overexpression was induced with 0.5 mM IPTG and $FeCl_2$ or $CoCl_2$ (Table 2), for 4 hours at room temperature.

Cells were harvested by centrifugation at 7000 xg, for 10 min at 4 ºC, and resuspended in 20 mM Tris-HCl, pH 7.5 and 5 % glycerol (buffer A).

Table 2 - Protein overexpression metals supplements. All metals were used at 100 mM.

	***Kc* SOR Fe**	***Kc* SOR Co**	***Kc* SOR Ni**	***Af* SOR Fe**	***Af* SOR Co**	***Af* H46S Fe**	***Af* H46S Co**	***Kc* S70H**
Before induction	$FeCl_2$	$FeCl_2$	$FeCl_2$	$FeCl_2$	$CoCl_2$	$FeCl_2$	$CoCl_2$	$FeCl_2$
Induction	$FeCl_2$	$FeCl_2$ + $CoCl_2$	$FeCl_2$ + NiCl2	$FeCl_2$	$CoCl_2$	$FeCl_2$	$CoCl_2$	$FeCl_2$

3.4. Purification

All purification steps were performed at 4 °C. The cells were lysed in a French press apparatus at 16000 psi. Cell lysate was cleared by two centrifugation steps at 25000 x*g* and 138000 x*g* to eliminate non-lysed cells and cell debris and membrane fraction, respectively.

Fraction containing the desired protein was dialyzed, in a 12-14 kDa cut-off dialysis membrane, overnight against buffer A and loaded into a DEAE column (GE Healthcare) previously equilibrated with buffer A. A linear gradient from 0 to 30 % of 20 mM Tris-HCl (pH 7.5) and 5 % glycerol and 1 M NaCl (buffer B) was applied to isolate the desired protein from other contaminants. The purity of the fractions containing the desired protein was verified by SDS-PAGE, and UV-Visible spectroscopy.

They were then pooled and concentrated in a diaflow apparatus with a 10 kDa cut-off membrane.

A second purification step was applied using a Superdex 75 column (GE Healthcare) previously equilibrated with 20 mM Tris-HCl, pH 7.5 and 5 % glycerol and 150 mM NaCl (buffer C). Again, purity and presence of the fractions containing the desired protein was verified by SDS-PAGE, and UV-Visible spectroscopy.

3.5. Biochemical characterisation

3.5.1. Protein quantification - Bradford protein assay:

The Bradford protein assay is a colourimetric procedure[70] used to determine the concentration of protein in a solution. It is a very sensitive assay, with a detection limit of 0.01 mg protein/ml. This method is based on the binding of the dye Coomassie Brilliant Blue G-250 to protein. Under acidic conditions, the dye is red and double protonated. Upon contact, the dye donates electrons to the protein which causes alterations in its structure, exposing hydrophobic pockets. These are stabilised by the dye acidic groups, resulting in a shift of its absorption maximum from 465 to 595 nm, and the protein-dye complex turns blue. As this complex is directly proportional to the amount of protein in solution, the concentration of protein can be determined by measuring the absorbance at 595 nm. This method uses bovine serum albumin (0.5 mg/ml) to build a calibration curve between 0 and 7.5 mg of protein (Appendix 5). For each protein, 2 samples with different volumes and duplicates were prepared to decrease the error margin of the method.

3.5.2. Inductively coupled plasma atomic emission spectroscopy

Initially the iron quantification was determined by following a spectrophotometric procedure, making use of a calibration curve with an Fe standard. However, this procedure was not efficient to determine the concentration of metals present in solution and, instead, protein samples were sent to ICP-AES in order to determine metals contents.

3.5.3. Quaternary structure

In order to determine the quaternary structure of the *Korarchaeum cryptofilum* SOR a size-exclusion chromatography was performed (Superdex 200 10/300, GE Healthcare). Molecular mass markers were used to determine a calibration curve (Appendix 6). The protein was loaded with blue dextran in order to mark the column void volume. The molecular mass of the proteins was calculated by:

$$Log_{10}(MM)_{Kc\ SOR} = Slope*V(eluted)+b; \qquad 3.1)$$

where, slope and b were derived from the calibration curve. The quaternary structure was determined by dividing the determined molecular mass by the theoretical one obtained from the amino acid sequence, 25 kDa.

3.5.4. SOD Activity – PAGE analysis

Protein activity was assessed by NATIVE-PAGE gel electrophoresis, in a 12.5 % acrylamide. NATIVE-PAGE gel was prepared without SDS or β-mercaptoethanol and was run at 120 volts at 4º C to prevent overheat. Once finished, the gel was washed with water and incubated for 20 minutes with 2.45 mM Nitrobluetetrazolium (0.2% w/v). It was again washed with water and incubated under a light source with a solution containing 0.28 mM TEMED (stock 6.6 M), 0.028 mM riboflavin and 0.36 mM buffer phosphate pH 7.8.

3.6. Spectroscopic characterisation

3.6.1. UV-Visible

UV-visible spectroscopy was used to obtain absorption spectra to monitor the state of the proteins after each purification step, in a PerkinElmer® Lambda 35 spectrophotometer. The measurements were performed with quartz cuvettes (Hëllma®) with 1 cm of path length at room temperature. Absorption spectra were obtained from 900 to 250 nm for each sample, with buffer solution A as blank or as a diluting agent. The results were then compared with the literature and between themselves.

3.6.2. Electron Paramagnetic Resonance

Electron Paramagnetic Resonance (EPR), is a magnetic resonance spectroscopic technique that detects species with unpaired electron, such as radicals, through microwave radiation in the presence of an externally applied static magnetic field. It is vastly used in the study of metalloproteins in order to understand their electronic proprieties and structure. An electron is a negatively charged particle with certain mass, with an associated spin. A magnetic moment of a molecule is primarily contributed by unpaired electron's spin magnetic moment. Applying a magnetic field to this magnetic movement, originates two different energy levels. By irradiating the electrons with a fixed microwave frequency equal to the energy gap between these two levels, this allows for a resonance condition and a transition of electrons in the lower energy level occurs to the upper energy level.

Electron paramagnetic resonance data used in this work were obtained using a Bruker EMX spectrometer with cooling equipment ESR-900 continuous flow helium cryostat (Oxford Instruments®) and a high sensitivity perpendicular mode rectangular cavity. The parameters to obtain the spectra were: Microwave power: 2 mW; Microwave frequency: 9.41 GHz; Amplitude modulation: 10 G; Protein concentration: 200 µM, temperature 4.3 and 20 K. EPR samples were prepared aerobically to a final concentration of 200 µM and stored in a Clear Fused Quartz (CFQ) tubes, which were kept in liquid nitrogen.

3.6.3. X-ray crystallography

X-ray crystallography is a technique used for determining the three-dimensional molecular structure from a crystal of a purified sample. Beams of X-rays are diffracted into specific directions by crystalline atoms and by measuring the angles and intensities of these diffracted beams, a crystallographer can produce a 3D picture of the density of electrons from the pattern of the diffraction spots.[71] The intensities of the spots can be used to determine the "structure factors" from which a map of the electron density can be calculated. The quality of the map is then improved, through various methods, to permit the building of the molecular structure using the protein sequence. The resulting structure is then refined to fit the map more accurately and to adopt a thermodynamically favoured conformation.

Korarchaeum cryptofilum SOR samples were subjected to size exclusion chromatography (Superdex 75 10/300 GE Healthcare) prior to crystallisation trials to isolate a single oligomeric state. They were then pooled and concentrated in a diaflow apparatus with a 10 kDa cut-off membrane until reaching 15 mg/mL. Crystallisation screens were setup using structure 1 and 2 (Biogenova) solutions, in a protein crystallisation robot – mosquito LCP - with round-bottom Greiner 96-well CrystalQuick™ plates (Greiner Bio-One) and stored at room temperature and at 4 ºC.

Korarchaeum cryptofilum SOR supplemented with iron, condition #G2 (0.2 M ammonium sulfate, 0.1 M MES, pH 6.5, 30% w/v PEG 5000 MME) and *Archaeoglobus fulgidus* SOR mutant, H46S supplemented with cobalt, condition #G6 (1.0 M Lithium sulfate, 0.1 M Sodium citrate, pH 5.6), were optimized in 2 µL sitting drops in vapor diffusion with 500 µL reservoir solution, using XRL 24-well crystallisation plates (Molecular Dimensions), at 20 ºC and 4 ºC and varying the pH and PEG (%). For the trips to the synchrotron sources the samples were frozen in liquid nitrogen with 20 % glycerol and 20 % ethylene glycol.

4. Results

4.1. *Korarchaeum cryptofilum* SOR

4.1.1. Expression tests and overexpression

Expression tests were conducted to determine the optimal conditions for *Kc* SOR overexpression. Two groups of samples were induced with four different IPTG concentrations (0 as the negative control, 0.1, 0.5 and 1 mM) at OD_{600nm} 0.5 or OD_{600nm} 0.9. Since the catalytic site of superoxide reductases contains iron, these expression tests were performed with iron supplementation. Samples were collected at three different time points at 4, 8 and 20 hours (overnight) after induction. The samples were analysed by SDS-PAGE in order to observe the expression of the target protein (Fig. 16).

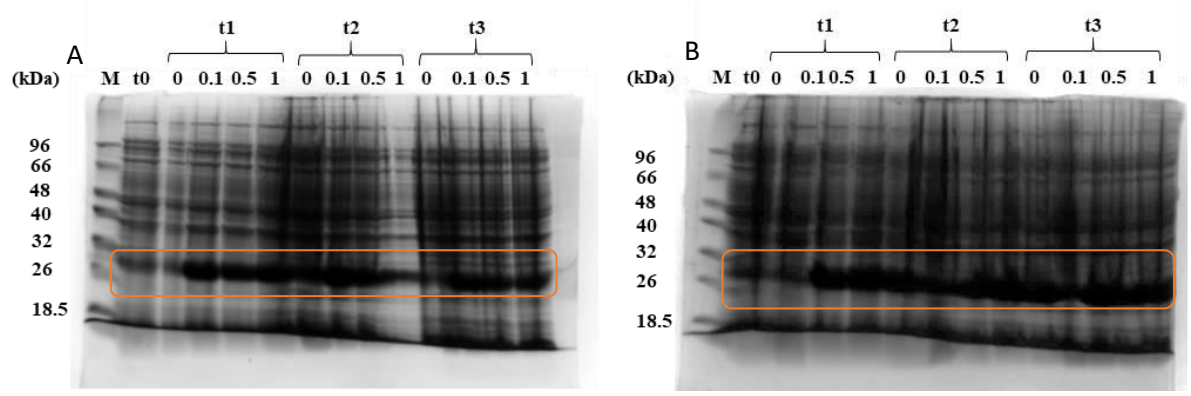

Figure 12 – SDS-PAGE analysis of *Korarchaeum cryptofilum* SOR expression tests; A- IPTG induction at OD_{600nm} 0.5; B- IPTG induction at OD_{600nm} 0.9; M – Marker, 0 – no IPTG induction (negative control), (0.1) 0.1 mM IPTG, (0.5) 0.5 mM IPTG, (1) 1 mM IPTG, (T1) 4 hours after IPTG induction, (T2) 8 hours after IPTG induction and (T3) Overnight after IPTG induction.

The cellular extract at t0 (A) shows a slight protein expression, and from t1 onwards, *i.e.*, after induction, an increase in protein expression is evident and remains constant, with the exception of 0 mM overnight. When induction is performed at OD_{600nm} 0.9, the protein expression pattern observed by SDS-PAGE is similar to that obtained for OD_{600nm} 0.5: protein expression is already visible at t0 and increases after induction. It was determined that the optimal conditions for protein overexpression were induction at OD_{600nm} 0.5 with 0.1 mM IPTG and four hours of incubation. As seen in Fig 16. A, induction at a lower optical density results in a cleaner background, compared to Fig. 16.B. The lowest concentration of IPTG was chosen since it yields a good level of protein expression (similar to that of the other conditions), as assessed by SDS-PAGE, and it avoids cell toxicity issues that may arise at higher concentrations.

Once the optimal conditions were determined the expression of *Korarchaeum cryptofilum* SOR was scaled-up. However, after the first batch it was determined that four hours incubation was insufficient and so the incubation period was increased to overnight and stayed as the standard condition onwards. After overnight expression, the culture medium started to exhibit a red colouration. A sample was analysed by SDS-PAGE in order to confirm protein expression at the established conditions (Fig. 17).

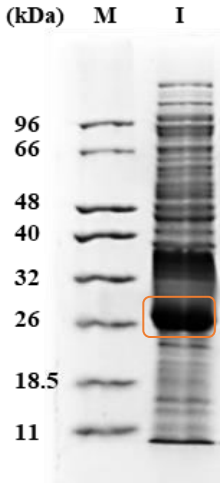

Figure 13 - SDS-PAGE analysis of *Korarchaeum cryptofilum* SOR cellular extract; (M) Marker, (I) *Kc* SOR 2 µL.

Kc SOR was overexpressed with four different metal supplements (cobalt, copper, zinc and nickel), in addition to iron supplement, under the conditions determined in the expression tests. The nickel and zinc supplemented cultures showed a similar faint yellow colouration, after cellular growth in the colourless M9 medium (Fig. 18). Similarly, to the iron supplemented culture, cultures supplemented with copper and cobalt presented a distinct colouration after overnight incubation, pink, orange and green respectively.

Figure 14 - *Korarchaeum cryptofilum* SOR overexpression with different metals supplements, (A) Iron and Copper, (B) Iron and Nickel, (C) iron, (D) Iron and Zinc and (E) Iron and Cobalt, after overnight induction with 0.1 mM IPTG.

Samples from each growth were applied to an SDS-PAGE to confirm protein expression. (Fig. 19).

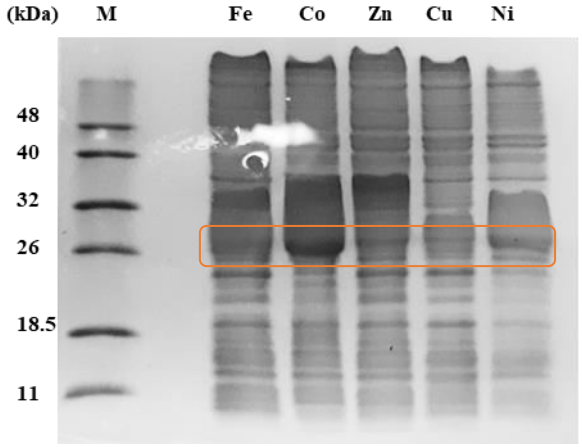

Figure 15 - SDS-PAGE analysis of *Korarchaeum cryptofilum* SOR overexpression with different metal supplements; (M) Marker, (Fe) *Kc* SOR supplemented with iron, (Zn) *Kc* SOR supplemented with iron and zinc, (Cu) *Kc* SOR supplemented with iron and copper, (Ni) *Kc* SOR supplemented with iron and nickel and (Co) *Kc* SOR supplemented with iron and cobalt.

4.1.2. Purification

The first step in the purification of *Kc* SOR supplemented with iron was an ionic exchange chromatography (Fig. 20 – see section 10.4 methods). Three different elution bands could be distinguished. The first peak, FI, comprises the samples eluted with 30 % of buffer B during the linear gradient, which had a red colouration as expected for the target protein. The second peak contains the samples eluted with further increase of buffer B concentration (FII).

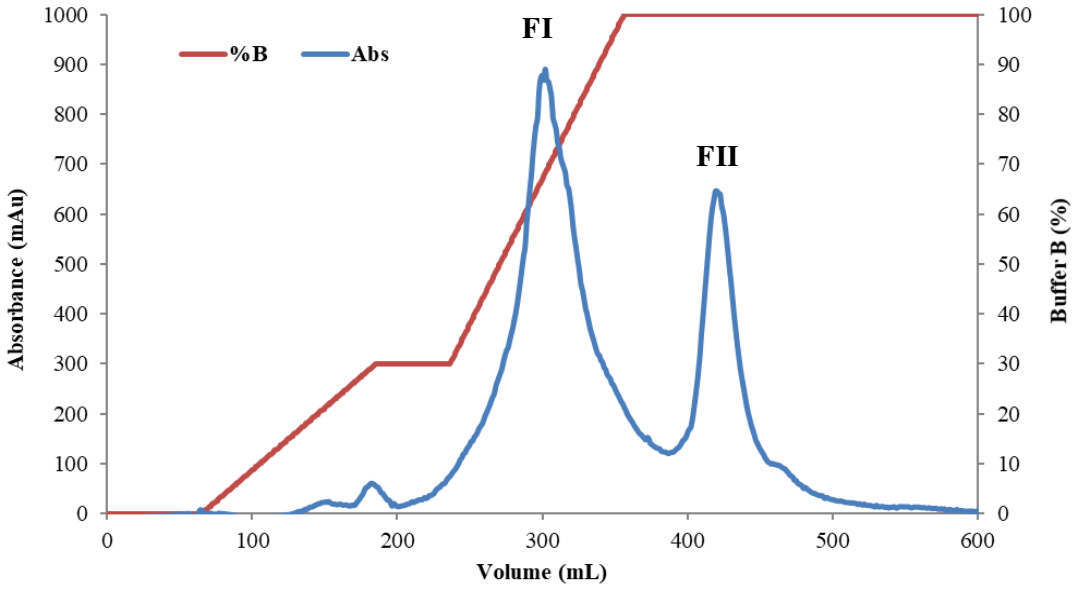

Figure 16 - Purification of *Korarchaeum cryptofilum* SOR supplemented with iron, by ion-exchange chromatography. The cell extract was loaded onto a DEAE column equilibrated with buffer A (20 mM Tris-HCl pH 7.5, 5% glycerol). SOR was eluted with a 0-30% linear gradient of buffer B (20 mM Tris-HCl pH 7.5, 5% glycerol and 1M NaCl): FI (target protein) eluted at 30% B and FII (residual protein with impurities) eluted at 40-60% B. At the end the column was washed with NaOH.

The relative amount and purity of the target protein in the fractions collected from the ion-exchange chromatography were assessed by SDS-PAGE (Fig. 21), and UV-visible spectroscopy. The SDS-PAGE analysis revealed the presence of the target protein in all fractions. Fraction I, presented a strong red colour which correlates with the high amounts of target protein observed in the gel. On the other hand, fraction II, and the wash elute exhibited weaker colouration which agrees with the residual levels of target protein detected by SDS-PAGE.

UV-visible spectroscopy analysis of fraction I showed two peaks at approximately 363 and 504 nm that are characteristic of charge-transfer bands (cys-metal)[72] for an oxidised desulforedoxin centre with iron incorporated (centre I).[34]

Following ion-exchange chromatography, further sample purification was achieved by size-exclusion chromatography using a Superdex 75 column for FI. Three peaks can be observed in the corresponding chromatogram (Fig. 21).

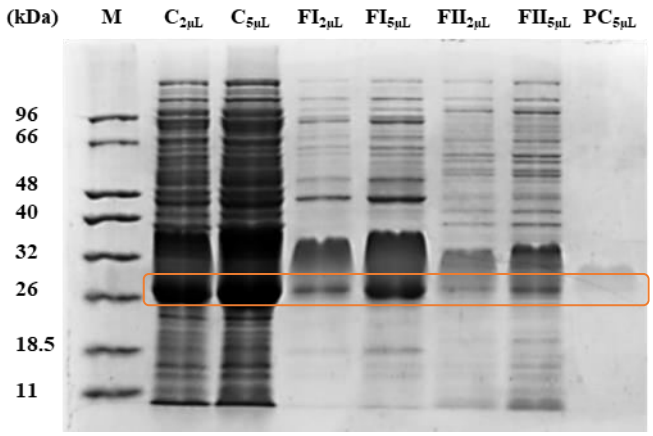

Figure 17 - SDS-PAGE analysis of *Korarchaeum cryptofilum* SOR supplemented with iron, before and after ion-exchange chromatography. (M) Markers, (C) Soluble fraction, (FI) Fraction I (peak A), (FII) Fraction II (peak B) and (PC) Fraction eluded with NaOH. Peak A presented more protein amount in comparison with peak B which presented residual protein and in fraction eluded with NaOH faint traces of residual protein could be observed.

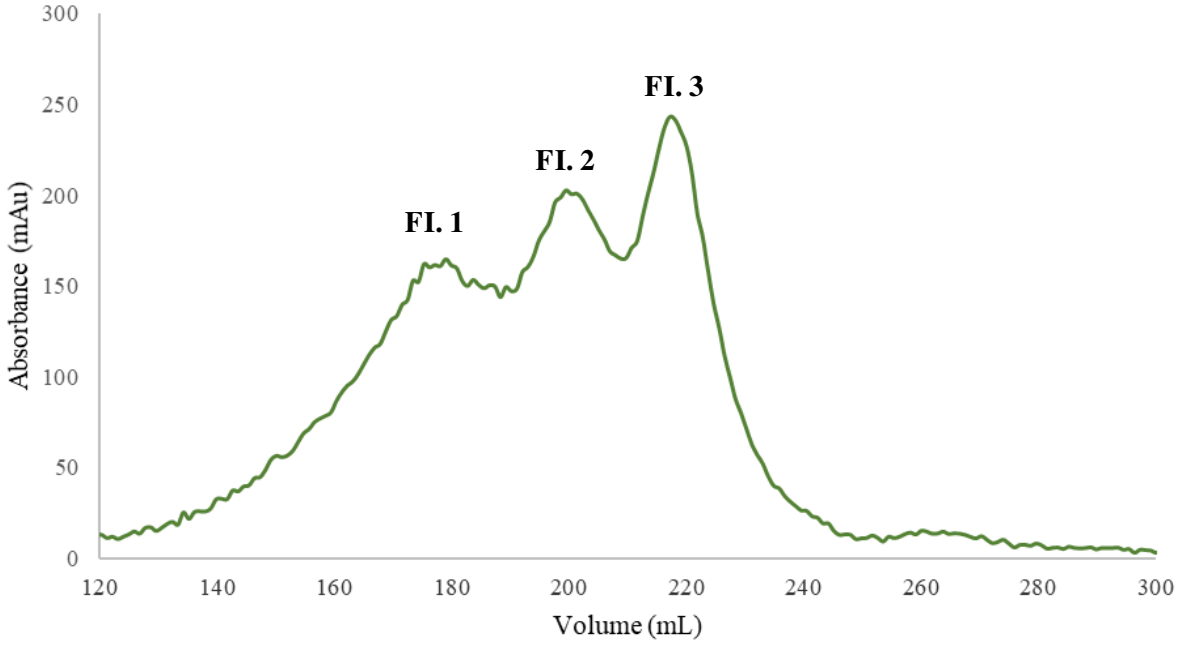

Figure 18 - Purification of *Korarchaeum cryptofilum* SOR supplemented with iron, by SEC. *Kc* SOR supplemented with iron was loaded in a S75 column previously equilibrated with buffer C (20 mM Tris-HCl, pH 7.5 and 5 % glycerol and 150 mM NaCl.).

Since the three fractions retrieved from SEC showed similar UV-Visible spectra (Fig. 23) the 280/495 nm absorbance ratio was used to determine their relative purity (Table 3); this allowed the identification of FI.3 as the purest fraction. Moreover, the peaks observed may be indicative of different oligomeric states of the protein.

Two peaks corresponding to an oxidised desulforedoxin centre (centre I)[27] were observed at approximately 360 and 530 nm (Fig 23). To assess if the neelaredoxin centre was in a reduced state,[27] the sample was oxidised with hydrogen peroxide (100 mM). No alterations were observed which may indicate lack of iron in the neelaredoxin centre or the presence of a different metal. At this stage, the *Kc* SOR presented a red colour.

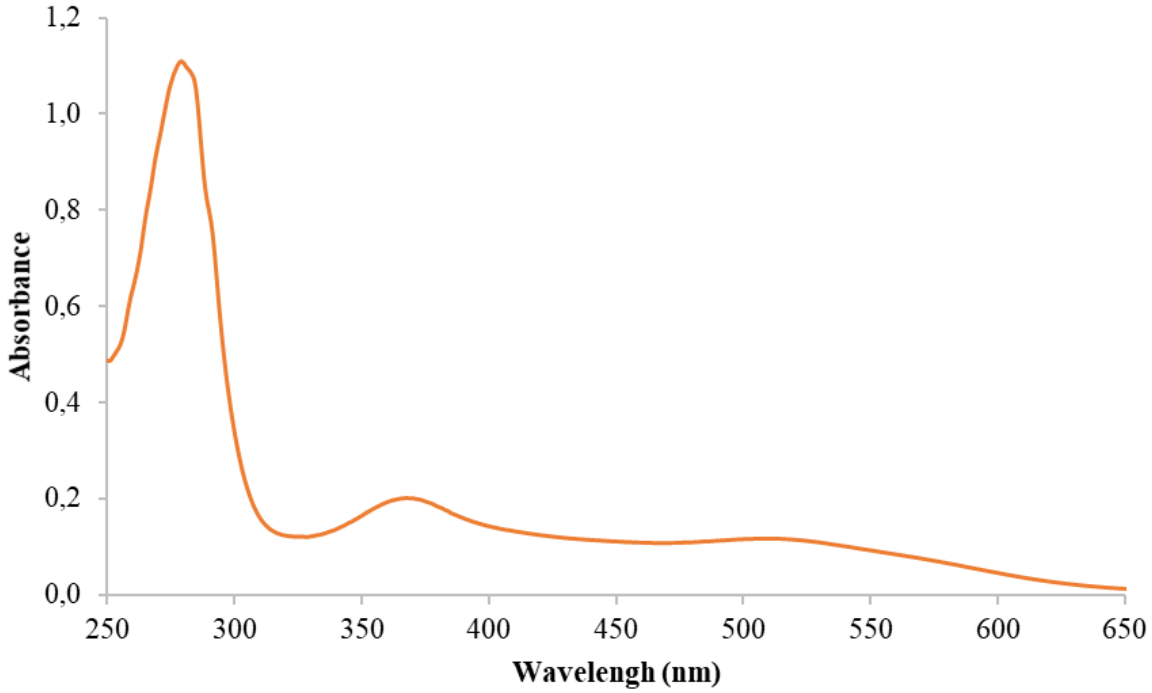

Figure 19 - UV-visible spectrum of *Korarchaeum cryptofilum* SOR supplemented with iron, as purified.

Table 3 - UV-visible peaks and A280/495 nm ratio for *Korarchaeum cryptofilum* SOR after SEC

Peak	Vial	λ280	λ495	Ratio 280/495
FI. 1	7	0.70	0.03	23
	10	0.67	0.05	13
FI. 2	13	0.90	0.06	15
	16	0.80	0.05	16
FI. 3	18	1.05	0.12	9
	19	0.73	0.07	10
	20	0.47	0.04	13

Moreover, given the results of the ratio analysis, fraction FI.3 was also analysed by SDS-PAGE (Fig. 24).

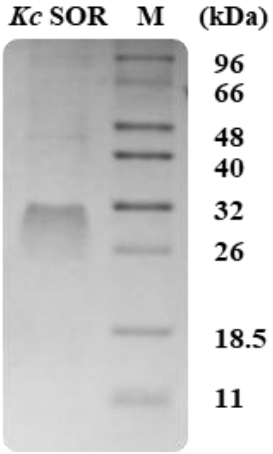

Figure 20 - SDS-PAGE analysis of *Korarchaeum cryptofilum* SOR, supplemented with iron, as purified. (M) Markers.

The remaining proteins described in this work were submitted to the same purification scheme outlined above, *i.e.,* ionic exchange chromatography, followed by size exclusion and monitored by UV-visible and SDS-PAGE analysis.

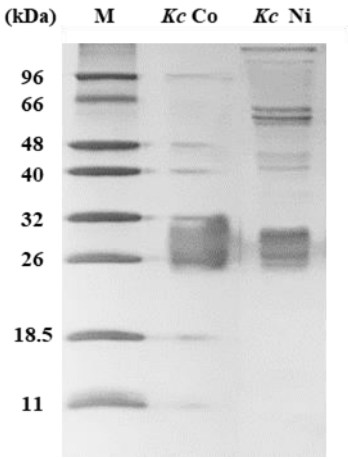

Figure 21 - SDS-PAGE analysis of *Korarchaeum cryptofilum* SOR. (M) Markers, (Co) *Kc* SOR supplemented with iron and cobalt, (Ni) *Kc* SOR supplemented with iron and nickel.

4.2. *Archaeoglobus fulgidus* SOR and H46S mutant overexpression and purification

The overexpression of *Archaeoglobus fulgidus* wild type and H46S mutant, with the five different metal supplements (the same used for *Kc* SOR overexpression), gave rise to distinct culture media colourations (Fig. 26). Since this protein only has one metallic centre, a basal iron supplementation was not used to avoid metal competition. Instead, only a single supplementation with the metal of interest was performed. Similar to what was previously observed for *Kc* SOR, the cultures supplemented with cobalt and copper showed green and red colouration, respectively, and those supplemented with iron, zinc and nickel had a faint yellow colour. The purification steps were monitored by UV-visible and SDS-PAGE (Fig. 27).

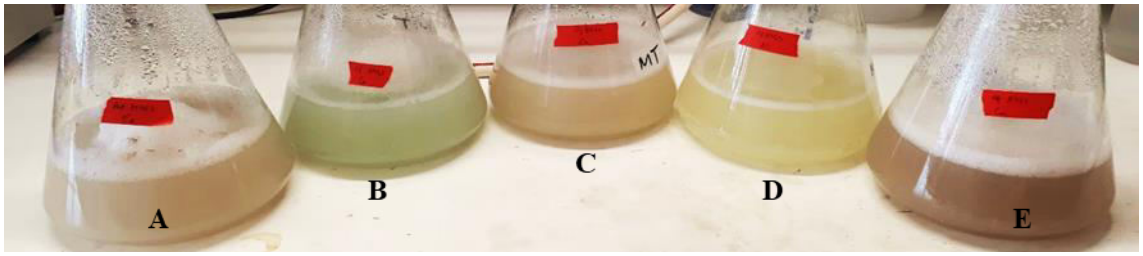

Figure 22 - *Archaeoglobus fulgidus* mutant H46S, overexpression with different metals supplements, (A) Iron, (B) Cobalt, (C) Zinc, (D) Nickel and (E) Copper, after four hours induction with 0.5 mM IPTG

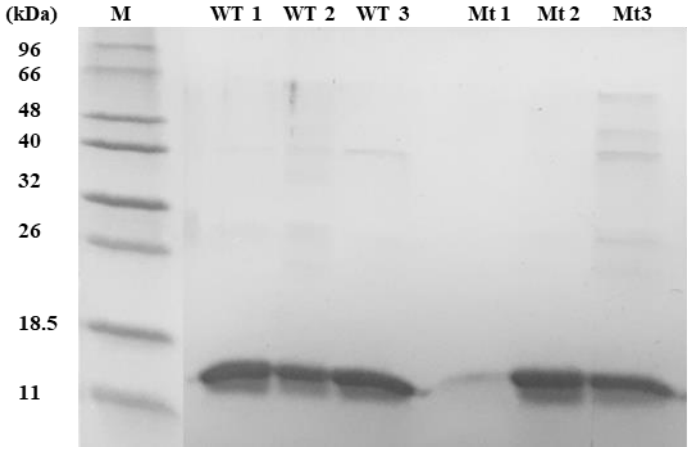

Figure 23 - SDS-PAGE analysis of *Archaeoglobus fulgidus* SOR and mutant H46S. (M) Markers, (WT 1) *Af* SOR supplemented with iron, (WT 2) cobalt, (WT 3) or nickel, and (Mt 1) *Af* H46S supplemented with iron, (Mt 2) cobalt, (Mt 3) or nickel.

After the purification steps, the amount of protein obtained for those supplemented with zinc and copper, namely *Kc* SOR and *Af* SOR wild-type and mutant, was not sufficient to carry on further studies.

4.3. Biochemical characterisation

4.3.1. Total protein quantification

Protein quantification was performed following the Bradford protocol (appendix 5).

Table 4 - Total protein quantification by the Bradford assay. The wild-type and mutant SOR proteins of *Kc* and *Af*, expressed with different metal supplements, were quantified after purification.

Proteins		Concentration (mM)	Amount (mg)
***Kc* SOR**	Fe	0.68 ± 0.08	289.10 ± 14.9
	Co	0.44 ± 0.01	11.01 ± 0.3
	Ni	0.08 ± 0.03	2.36 ± 0.1
***Kc* S70H**	Fe	0.07 ± 0.02	8.30 ± 0.4
***Af* SOR**	Fe	1.67 ± 0.01	91.51 ±0.5
	Co	0.04 ± 0.00	1.92 ±0.1
	Ni	0.03 ± 0.01	4.46 ± 0.8
***Af* H46S**	Fe	0.01 ± 0.00	0.14 ± 0.04
	Co	0.60 ± 0.03	123.65 ± 5.7
	Ni	0.02 ± 0.00	0.44 ± 0.05

4.3.2. Metal quantification (ICP-AES)

The metal content of the purified proteins was determined by ICP analysis. (table 5). The results indicate that the *Korarchaeum cryptofilum* SOR supplemented with iron has approximately 1.4 ± 0.12 iron atoms per protein. This can be explained either by a mix population of proteins in which some have incorporated iron into both centres, despite this not being visible in the UV-visible spectra data, or by an overestimation given that the values fall outside of the linearity range of the assay calibration curve. For *Kc* SOR supplemented with iron and cobalt, the results are consistent with cobalt incorporation in one centre and no incorporation of iron. The incorporation of iron in the iron supplemented *Kc* SOR S70H mutant was very low, with only about 0.3 ± 0.01 iron atoms per protein. *Archaeoglobus fulgidus* SOR supplemented with iron was determined to have less iron than expected, approximately 0.55 ± 0.07 iron atoms per protein instead of 1, although this is still representative of iron incorporation in the canonical neelaredoxin centre. On the other hand, the *Af* H46S mutant supplemented with cobalt shows good incorporation of the metal, with approximately 0.91 ± 0.12 cobalt atoms per protein, at the non-canonical neelaredoxin centre.

Table 5 - ICP analysis of SOR proteins supplemented with iron and/or cobalt. The metal content per protein was determined for *Korarchaeum cryptofilum* SOR wild-type supplemented with iron and with both iron and cobalt, *Kc* SOR S70H mutant supplemented with iron, *Archaeoglobus fulgidus* SOR wild-type supplemented with iron and *Af* H46S mutant supplemented with cobalt. Error values are negligible and thus are not presented.

SOR	Iron per Protein	Cobalt per Protein	Zinc per protein
***Kc* WT Fe**	1.40 ± 0.12	0.00	0.05
***Kc* WT Co**	0.04	0.37 ± 0.01	0.05
***Kc* S70H Fe**	0.27 ± 0.01	0.00	0.07
***Af* WT Fe**	1.60 ± 0.19	0.00	0.01
***Af* /WT Co**	ND	ND	ND
***Af* H46S Fe**	ND	ND	ND
***Af* H46S Co**	0.19 ± 0.02	0.91 ± 0.12	0.03

4.3.3. Quaternary structure

The quaternary structure of *Korarchaeum cryptofilum* SOR supplemented with iron was determined by gel filtration. Proteins of known molecular mass were used as standards (Appendix 6) to calculate a calibration curve, used to determine the molecular mass of the eluted SOR oligomers (table 6). Protein was eluted in two peaks (Fig 28), consistent with the formation of SOR dimer, expected for SOR[27] and hexamer, which may suggest some tendency for protein aggregation. This had already been observed during purification, in the size-exclusion chromatography.

Table 6 - Determination of Korarchaeum *cryptofilum* SOR quaternary structure by SEC. Markers and protein data retrieved from SEC performed in a S200 column. (For calculations used see Methods 3.5.3 section)

Sample	$V_{elution}$ (mL)	MM (kDa)	Subunits
Dextran Blue	8.72	2000	-
***Kc* SOR Fe**	12.60	147.4	6
	14.70	58.4	2

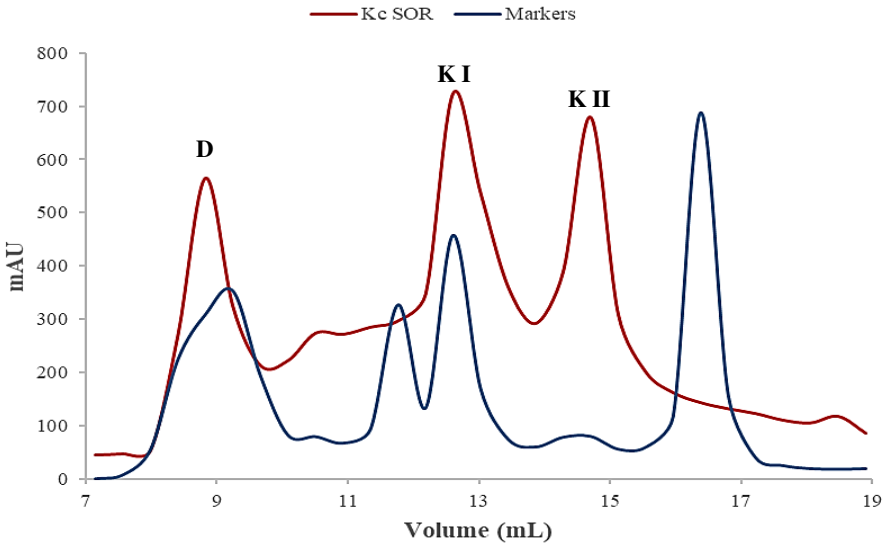

Figure 24 - *Korarchaeum cryptofilum* SOR vs Markers in gel filtration S200 column. (D) Dextran blue, (K I) *Kc* SOR eluted at 12.60 mL, (K II), *Kc* SOR eluted at 14.70 mL. Dextran blue was used as control marker.

4.4. Spectroscopic characterisation

4.4.1. UV-Visible

UV-Visible spectroscopy study was performed to evaluate the success of metal incorporation in all the proteins described in this work. To analyse the oxidation ability of the SOR catalytic centre with iron, two UV-visible spectra were registered: one with the protein as purified and other after incubation with hydrogen peroxide (100 mM).

4.4.1.1. *Korarchaeum cryptofilum* SOR

4.4.1.1.1. Iron supplementation

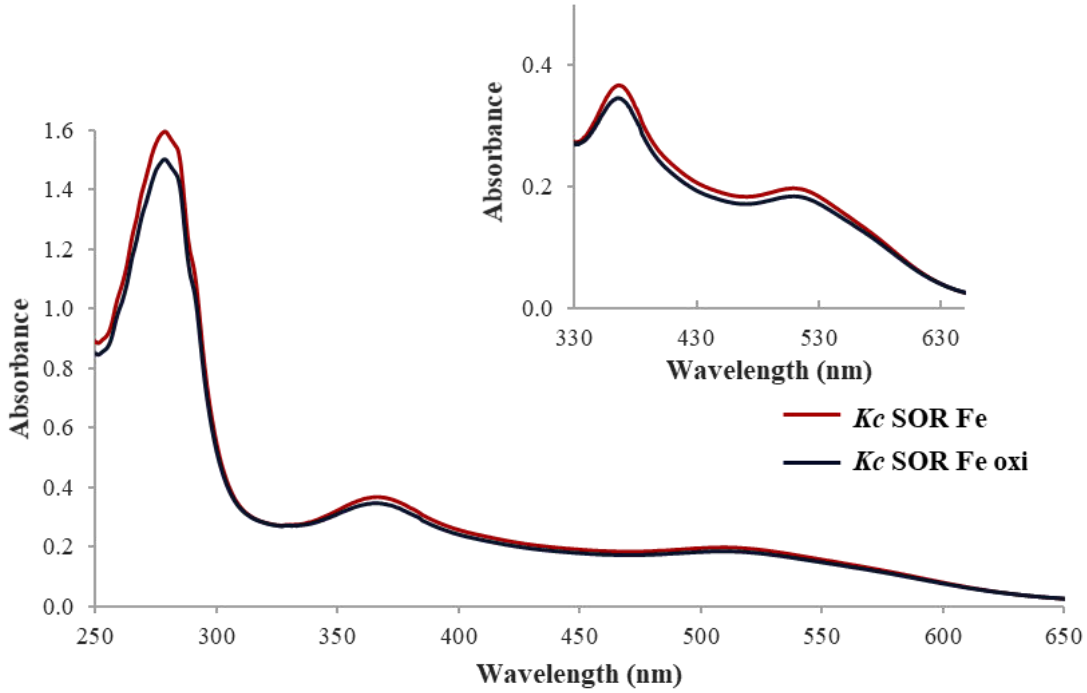

Figure 25 - UV-visible spectra of *Korarchaeum cryptofilum* SOR supplemented with iron (red) and oxidised with 100 mM hydrogen peroxide (blue). The inset represents a 4x zoom of the spectrum.

In the spectrum of *Korarchaeum cryptofilum* SOR supplemented with iron (Fig. 25), two bands were observed at approximately 360 and 530 nm, corresponding to an oxidised desulforedoxin centre.[27] Hydrogen peroxide (100 mM) was added to promote the oxidation of a possibly reduced non-canonical neelaredoxin centre: the spectrum of the oxidised sample revealed no significant changes, which may indicate lack of iron in the neelaredoxin centre or the presence of a different metal.

4.4.1.1.2. Iron and cobalt supplementation

Kc SOR supplemented with iron and cobalt (faint blue) was submitted to the same purification steps and rigorous analysis as the *Kc* SOR supplemented with iron. The spectrum of the purified protein (Fig. 26) shows absorption bands at 340, 529, 611, 631 and 722 nm. The first peak corresponds to the cysteine to metal charge transfer,[73] while the latter results from ligand field transitions (d-d).[26,74]

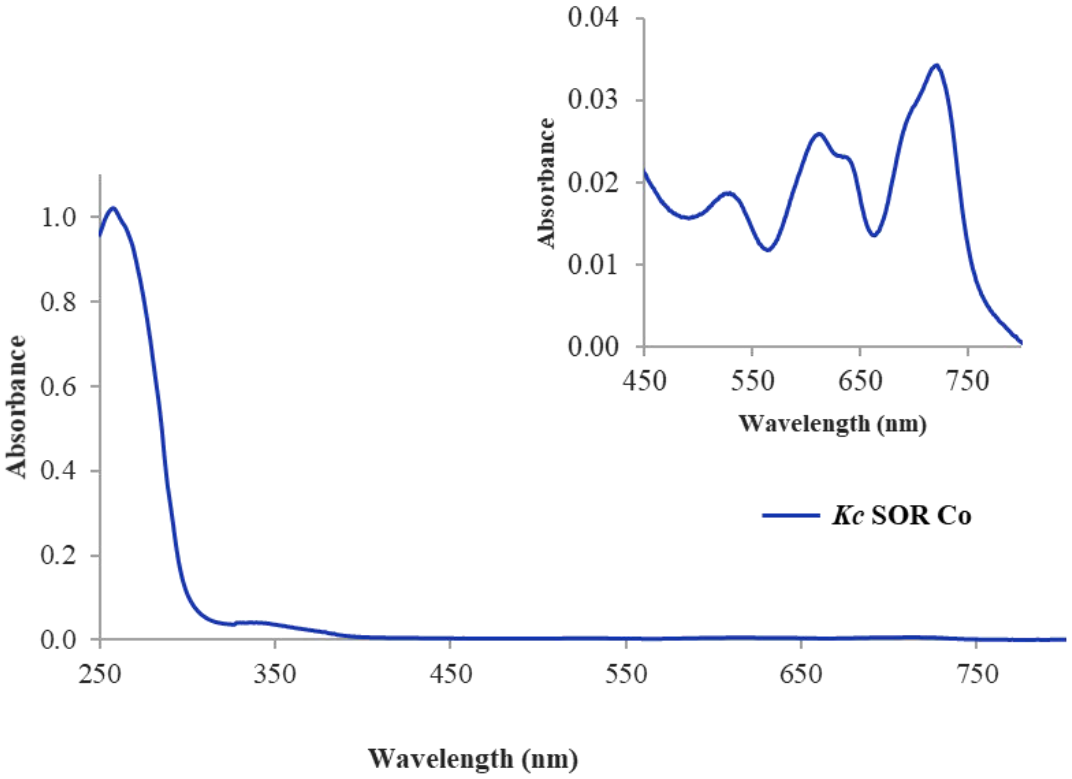

Figure 26 - UV-visible spectra of *Korarchaeum cryptofilum* SOR supplemented with iron and cobalt, as purified. The inset represents a 25x zoom of the spectra of a 5x more concentrated sample.

4.4.1.2. *Archaeoglobus fulgidus* SOR

4.4.1.2.1. Iron supplementation

The final spectrum of the purified *Af* SOR (Fig. 27), only supplemented with iron, shows a broad shoulder at *ca.* 300 and a band at 660 nm corresponding to the neelaredoxin centre; this sample presented a blue colour. The spectrum of the oxidised protein (100 mM hydrogen peroxide) revealed a higher absorbance value at 300 and 660 nm, confirming the oxidation of the iron-containing neelaredoxin centre.[75,26] This result was to be expected as the *Af* SOR has a canonical neelaredoxin centre and can thus be used as a positive control.[25]

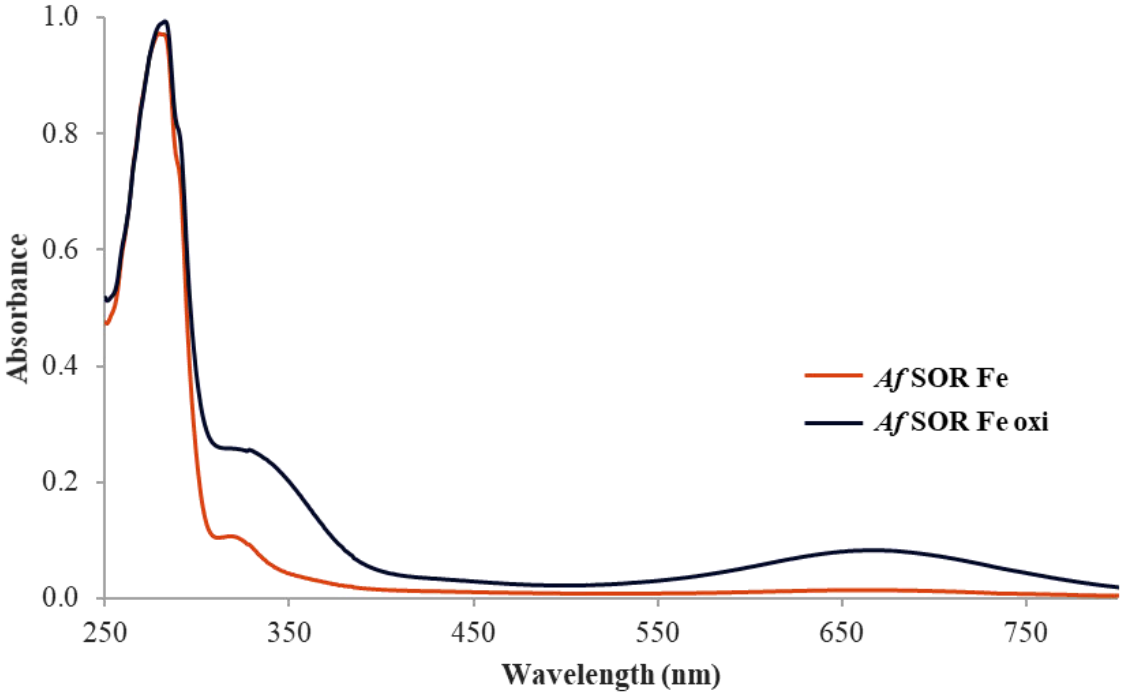

Figure 27 - UV-visible spectra of *Archaeoglobus fulgidus* SOR supplemented with iron. *Af* SOR, as purified (orange) and oxidised with 100 mM hydrogen peroxide (black).

4.4.1.2.2. Cobalt supplementation

The spectrum of the purified *Af* SOR with cobalt supplementation (Fig. 28), revealed no well-defined peaks but rather one shoulders at *ca.* 350 nm; this sample had no colour. No characteristic peaks for cobalt incorporated in the neelaredoxin centre could be concluded.[26,74,76]

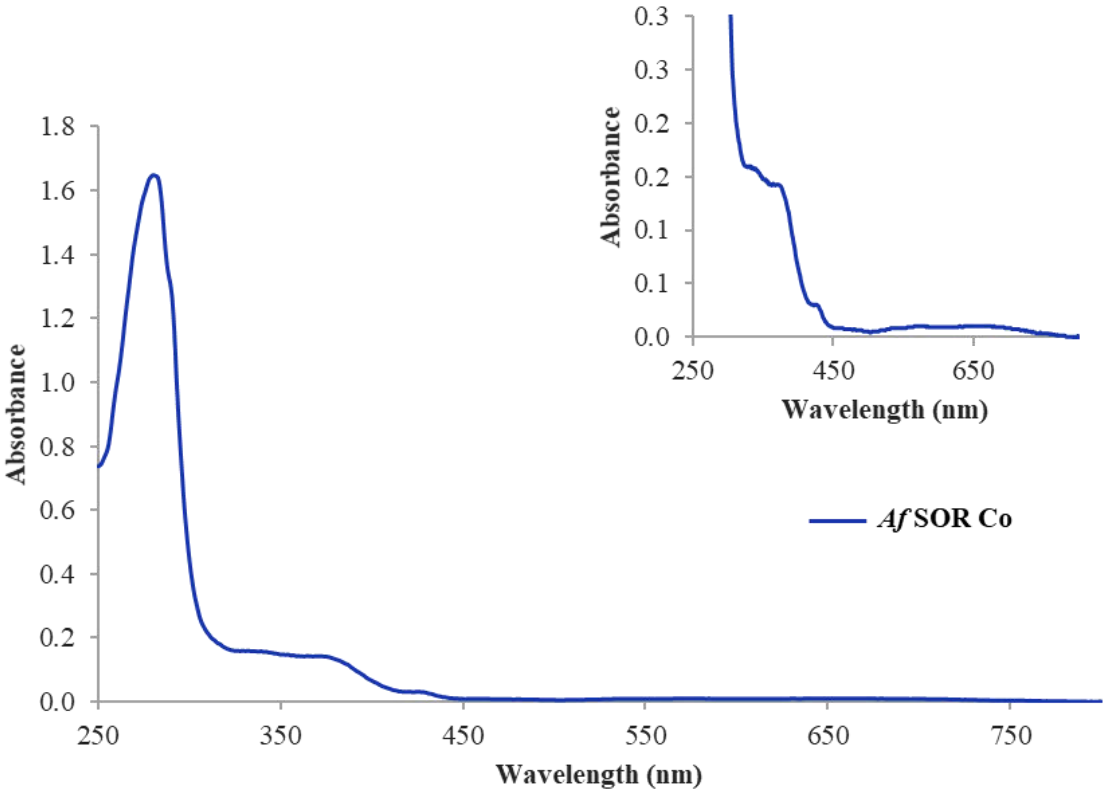

Figure 28 - UV-visible spectra of *Archaeoglobus fulgidus* SOR supplemented with cobalt, as purified. The inset represents a 6x zoom of the spectra.

4.4.1.3. *Archaeoglobus fulgidus* SOR H46S mutant

4.4.1.3.1. Iron supplementation

For the *Af* H46S mutant supplemented with iron, which is colourless, the spectrum of the purified sample exhibited no SOR related peaks (Fig. 29). The absence of iron in the non-canonical neelaredoxin centre may explain the UV-visible spectrum obtained. The *Af* H46S supplemented with iron was submitted to oxidization (100 mM hydrogen peroxide): it shows a lack of oxidation capabilities Furthermore, EPR data also indicates a lack of iron incorporation in the non-canonical neelaredoxin centre.

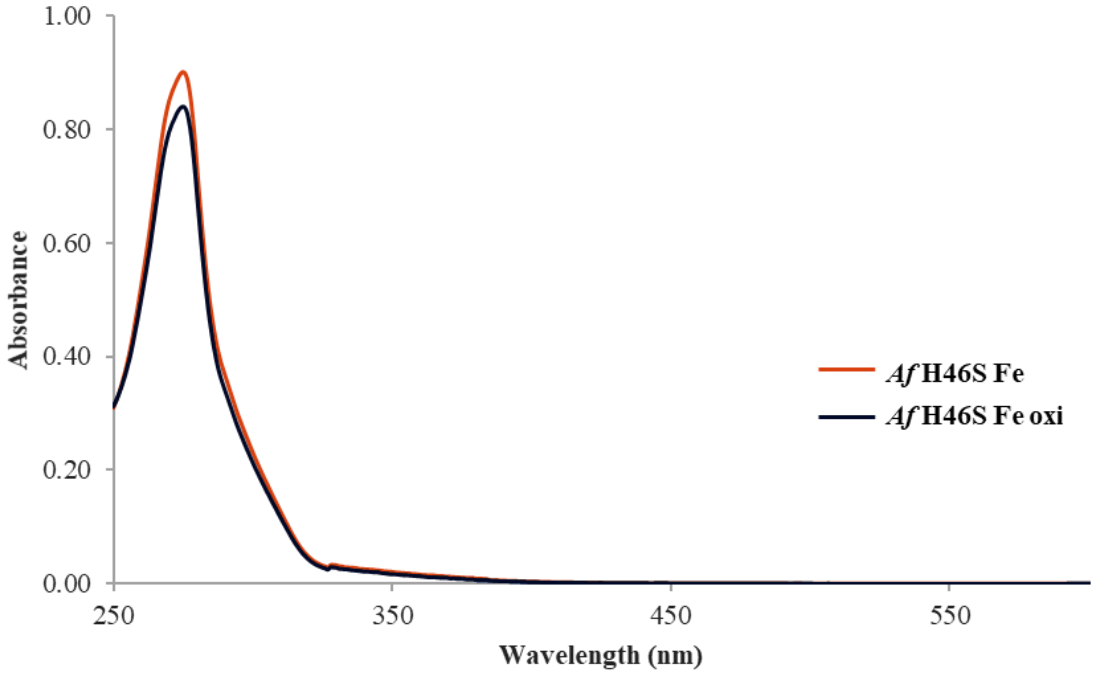

Figure 29 - UV-visible spectrum of *Archaeoglobus fulgidus* mutant H46S supplemented with iron, as purified (red), and oxidised with 100 mM hydrogen peroxide (black).

4.4.1.3.2. Cobalt supplementation

The *Af* H46S supplemented with cobalt had an evident blue colour and its UV-visible spectrum (Fig. 30), shows peaks at 350 nm 531, 617 nm and a shoulder at 649 nm corresponding to d-d transitions.[74] Together with the results from EPR and ICP, and since the *Af* H46S mutant only possesses the neelaredoxin centre, it can be concluded that the cobalt is successfully incorporated in the non-canonical neelaredoxin centre.

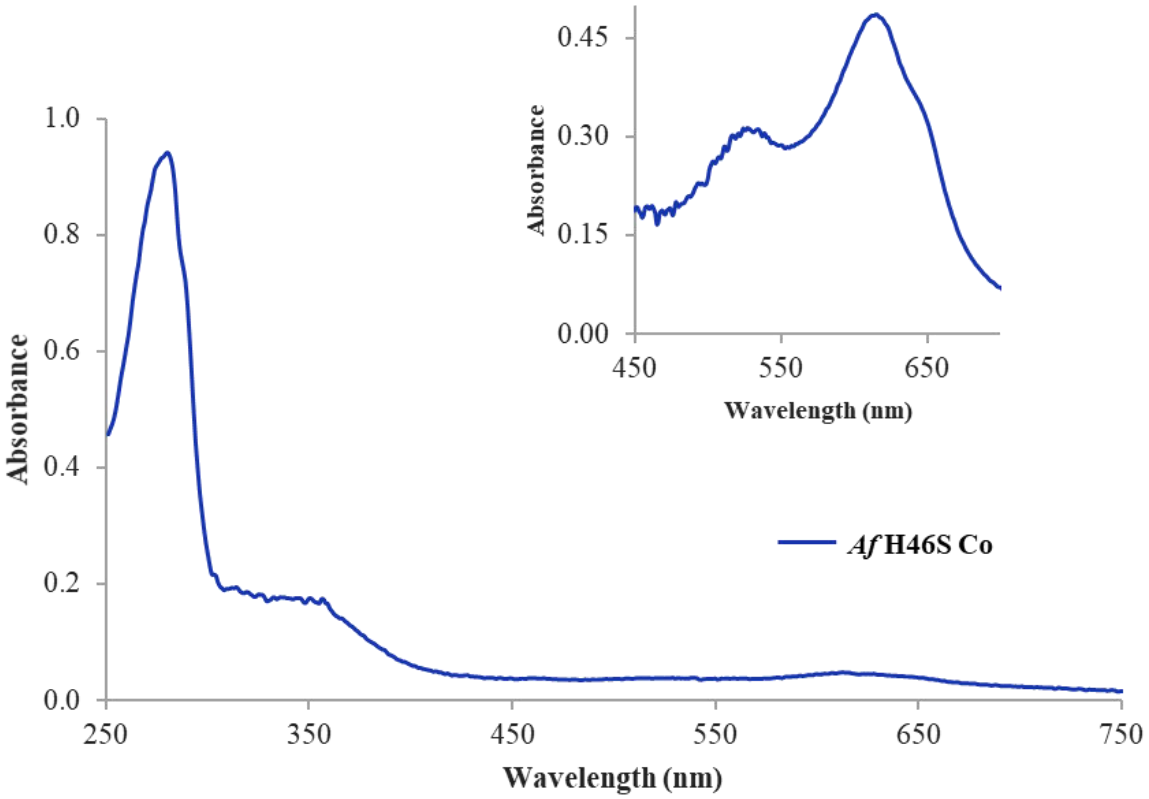

Figure 30 - UV-visible spectrum dil. 1:20**, of *Archaeoglobus fulgidus* H46S mutant supplemented with cobalt,** as purified**.** The inset represents a 2x zoom of the spectrum 1:1, between 450 and 700 nm.

4.4.1.4. *Korarchaeum cryptofilum* SOR S70H mutant

4.4.1.4.1. Iron supplementation

The *Korarchaeum cryptofilum* S70H mutant supplemented with iron was red like the *Kc* SOR supplemented with iron. The UV-visible spectrum (Fig. 42) shows two peaks associated with the oxidised iron-containing desulforedoxin centre at 360 and 530 nm. The spectrum showed no alterations upon protein oxidation with 100 mM hydrogen peroxide. Combined with the data from EPR studies, this indicates the lack of iron in the neelaredoxin centre.

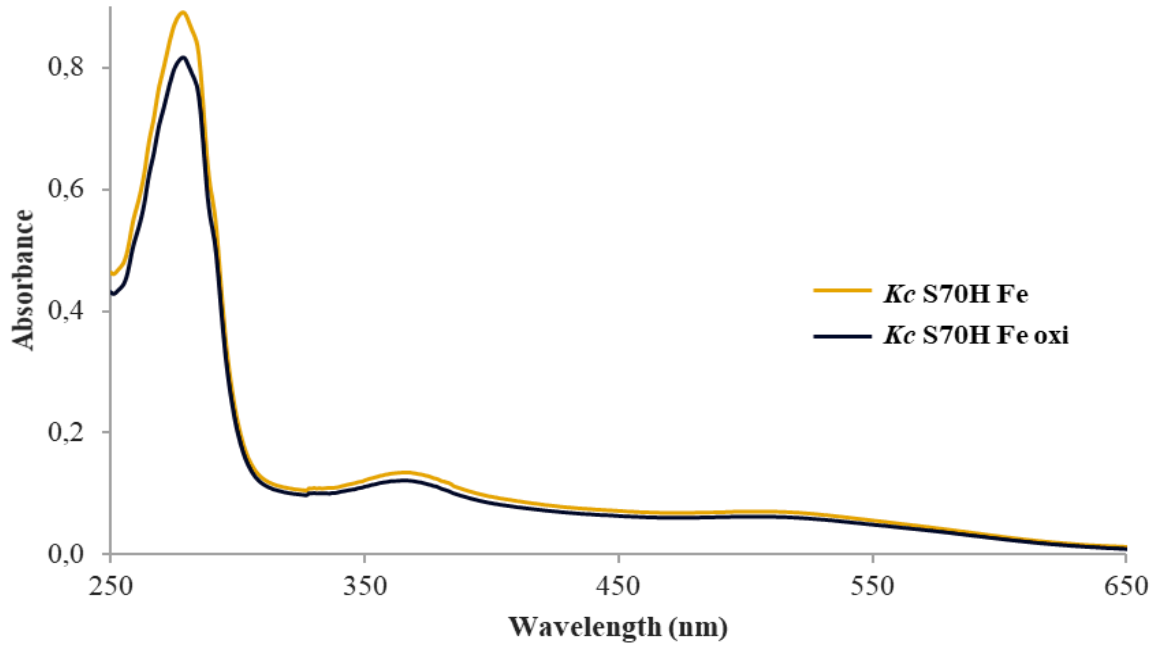

Figure 31 - UV-visible spectrum of *Korarchaeum cryptofilum* S70H mutant supplemented with iron, as purified (yellow) and oxidised with 100 mM hydrogen peroxide (black).

4.4.2. Electron Paramagnetic Resonance

EPR spectroscopy was performed to: study metal incorporation in the SORs described in this work and for comparison purposes. The EPR spectrum of *Korarchaeum cryptofilum* SOR supplemented with iron (Fig. 32) shows similarities with the EPR spectrum of desulforedoxin from *D. gigas*,[77] with iron incorporation in the desulforedoxin centre (centre I), with g values at 7.7, 5.6 and 4.2, which are almost identical to the desulforedoxin spectrum g values (7.7, 5.7 and 4.1).[77] For the non-canonical neelaredoxin centre (catalytic centre II) the characteristic features of the EPR spectrum were not observed.[78] This may be explained by the oxidation of the desulforedoxin centre and the reduction of the neelaredoxin centre, which is common for 2Fe-SOR proteins.[26] Nonetheless, this is in agreement with the UV-visible spectra, which already indicated the absence of centre II.

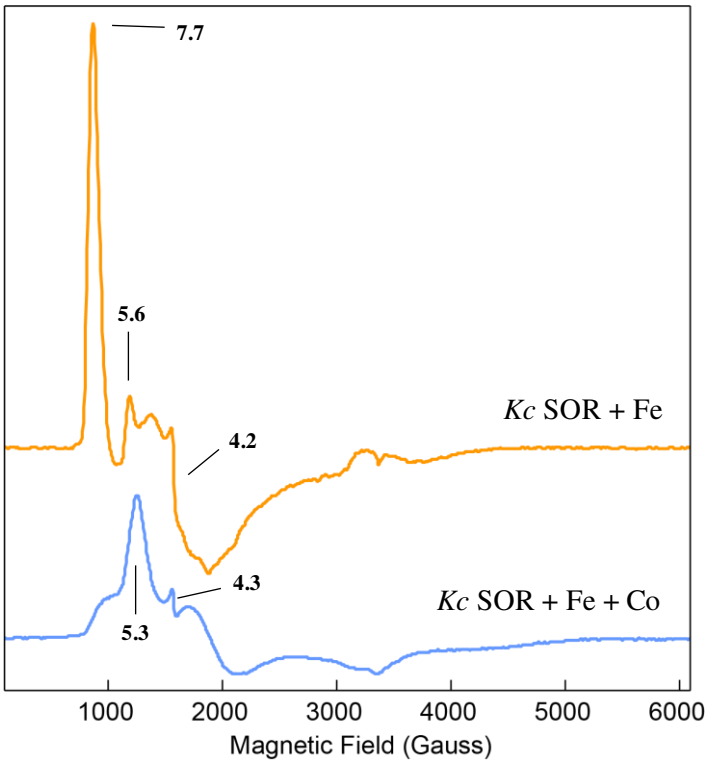

Figure 32 - EPR spectra for *Korarchaeum cryptofilum* SOR supplemented with iron (orange) **and *Kc* SOR supplemented with iron and cobalt** (blue) **at 4.3 K.** In the spectra the relevant g values are represented for each protein**.** Microwave power: 2 mW; Microwave frequency: 9.41 GHz; Amplitude modulation: 10 G; Protein concentration: 200 µM.

To confirm the lack of metal incorporation in the neelaredoxin centre of *Korarchaeum cryptofilum* SOR, the EPR spectrum of *Archaeoglobus fulgidus* SOR supplemented with iron was registered and compared with that of *Kc* SOR supplemented with iron (Fig. 33), The *Af* SOR supplemented with iron clearly yields g values at 7.0, 5.6 and 4.3, which are characteristic of an iron-containing neelaredoxin centre. These spectral features were not observed for *Kc* SOR supplemented with iron, that instead exhibited characteristics of a Dx centre,[74] which the *Af* SOR does not possess.

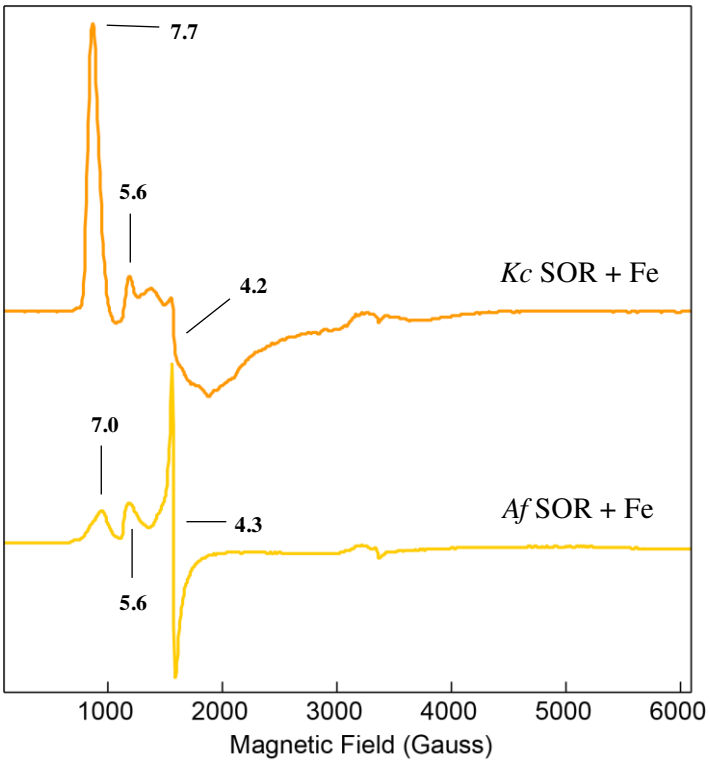

Figure 33 - EPR spectra of *Korarchaeum cryptofilum* SOR supplemented with iron (orange) **and *Archaeoglobus fulgidus* SOR supplemented with iron** (yellow) **at 4.3 K.** In the spectra the relevant g values are represented for each protein**.** Microwave power: 2 mW; Microwave frequency: 9.41 GHz; Amplitude modulation: 10 G; Protein concentration: 200 µM.

EPR spectra of *Kc* SOR supplemented with cobalt and *Archaeoglobus fulgidus* mutant, H46S supplemented with cobalt were compared (Fig. 34) With the exception of a broad shoulder at g~6.9 for the *Kc* SOR supplemented with cobalt, both spectra were comparable as both proteins successfully incorporated cobalt. Nonetheless, it was not possible to determine in which centre the cobalt was incorporated in the *Kc* SOR.[74] To determine if there was free cobalt in solution, the EPR spectrum of a cobalt chloride solution was acquired and, compared with the EPR spectra of *Kc* SOR Co and *Af* H46S SOR Co, confirming the cobalt incorporation in both proteins.

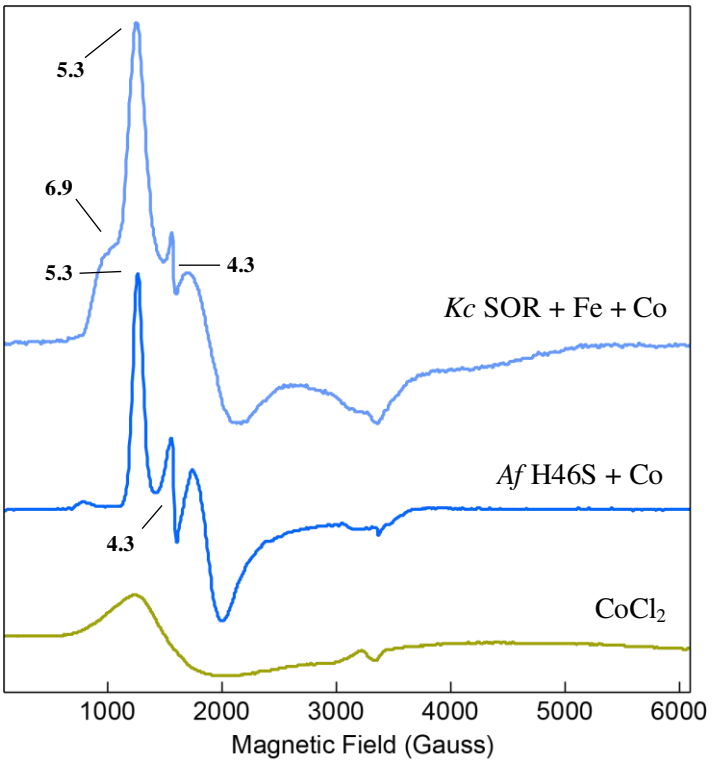

Figure 34 - EPR spectra of *Korarchaeum cryptofilum* SOR supplemented with iron and cobalt (light blue)**, *Archaeoglobus fulgidus* mutant H46S, supplemented with cobalt** (blue)**, and cobalt chloride solution** (green), **at 4.3 K**. In the spectra the relevant g values are represented for each protein. Microwave power: 2 mW; Microwave frequency: 9.41 GHz; Amplitude modulation: 10 G; Protein concentration: 200 µM.

To further understand the inability of iron incorporation in the non-canonical neelaredoxin centre, the EPR spectra of the *Korarchaeum cryptofilum* SOR S70H mutant, which has a canonical neelaredoxin centre similar to *Archaeoglobus fulgidus* SOR, was analysed. These spectra show similarities with that of *Kc* SOR supplemented with iron (Fig 32): the g values were almost identical with the exception of 4.2 for which the signal was stronger for *Kc* S70H. Considering the EPR spectra together with the UV-Visible spectra (Fig. 31) we can conclude that even with a canonical centre, the neelaredoxin centre of the *Kc* S70H was still incapable of incorporating iron. The *Af* H46S supplemented with iron, which has the same non-canonical neelaredoxin centre as *Kc* SOR, was used as control and no iron incorporation was observed, as g value at 4.3 was not characteristic for neelaredoxin centre with iron incorporated.

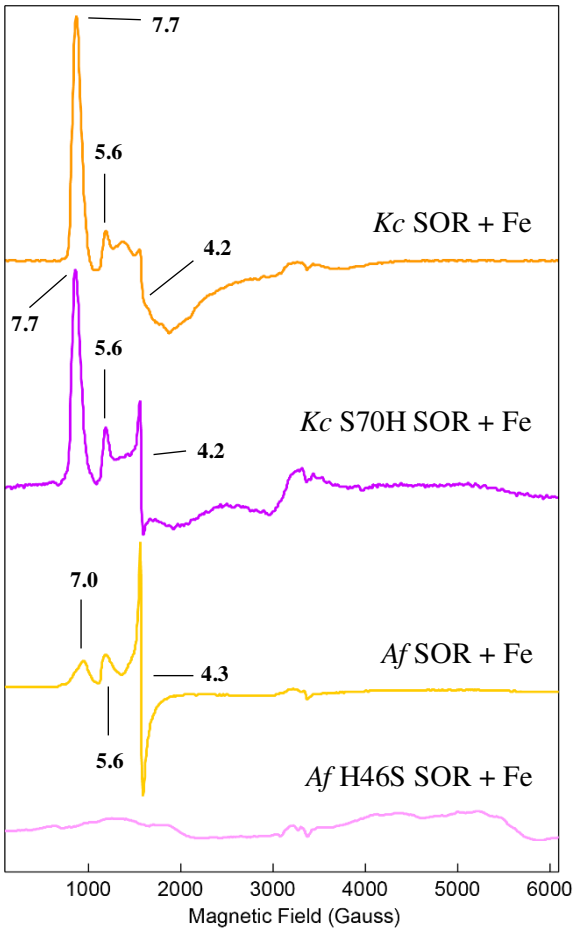

Figure 35 - EPR spectra of *Korarchaeum cryptofilum* SOR supplemented with iron (orange)**, *Kc* S70H mutant supplemented with iron** (purple)**, *Archaeoglobus fulgidus* SOR supplemented with iron** (yellow) **and *Af* mutant H46S, supplemented with iron** (pink), **at 4.3 K**. In the spectra the relevant g values are represented for each protein. Microwave power: 2 mW; Microwave frequency: 9.41 GHz; Amplitude modulation: 10 G; Protein concentration: 200 µM.

4.4.3. Native polyacrylamide gel electrophoresis (PAGE) – activity staining

To confirm if the proteins have the ability to use superoxide as substrate, two different staining methods were used after NATIVE-PAGE: Nitrobluetetrazolium (Fig. 43), and Coomassie (Fig. 44) staining. The native gel stained with NBT was used to identify proteins with activity. *Af* SOR supplemented with iron and superoxidase dismutase from bovine erythrocytes, were used as positive controls and BSA as a negative control. Wells A), B), E) and BSA did not shown signs of activity. In the positive control well (SOD) and *Af* SOR supplemented with iron, activity was observable. Moreover, in well D) (*Af* H46S supplemented with cobalt) little signs of activity were observed, however it was not conclusive, as contamination from well C) (*Af* SOR) could be the reason for some signs of dismutase activity in well D). From this gel it is possible to conclude that the *Korarchaeum cryptofilum* SOR supplemented with iron and with iron and cobalt, and the *Kc* S70H supplemented with iron have no activity. As for *Archaeoglobus fulgidus* H46S supplemented with cobalt more tests must be performed.

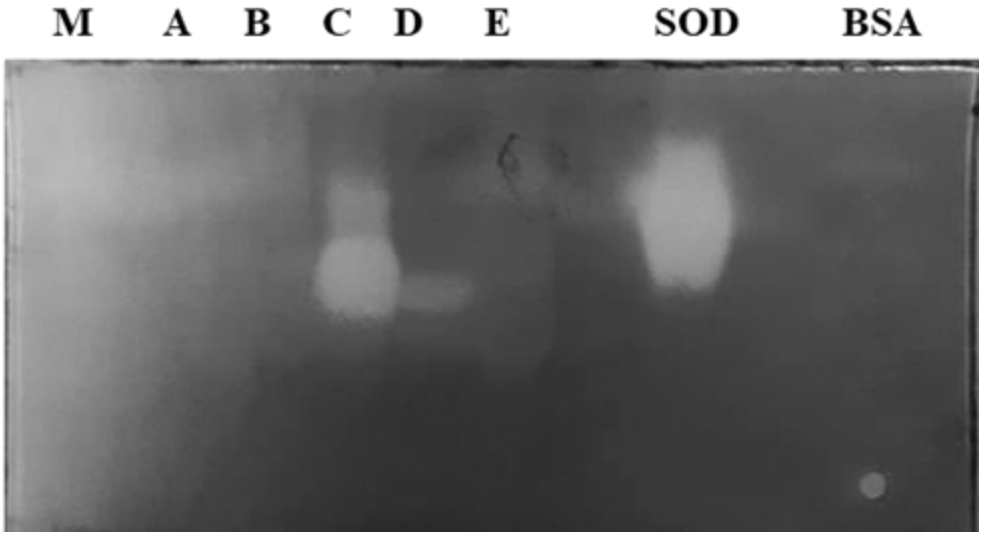

Figure 36 - NATIVE-PAGE followed by Nitrobluetetrazolium staining. (M) markers, (A) *Korarchaeum cryptofilum* SOR supplemented with iron, (B) *Kc* SOR supplemented with iron and cobalt, (C) *Archaeoglobus fulgidus* SOR supplemented with iron, (D) *Archaeoglobus fulgidus* H46S mutant supplemented with cobalt; (E) *Korarchaeum cryptofilum* S70H mutant supplemented with iron, (SOD) superoxidase dismutase 5 µg; (BSA1 mg/mL bovine serum albumin. Dismutase activity is observed for *Archaeoglobus fulgidus* SOR supplemented with iron (C) and for the superoxidase dismutase (SOD).

The second native gel was also stained with Coomassie (Fig. 44) in order to confirm the presence of the proteins. Being this a non-denaturing gel, mobility depends not only on the charge-to-mass ratio, but also on the physical shape and size of the protein. The results were as excepted, as the bands corresponding to *Korarchaeum cryptofilum* (A, B and E) had a similar migration pattern. For the *Archaeoglobus fulgidus* (well C) a larger band was observed, however it is in pair with *Af* H46S in well D).

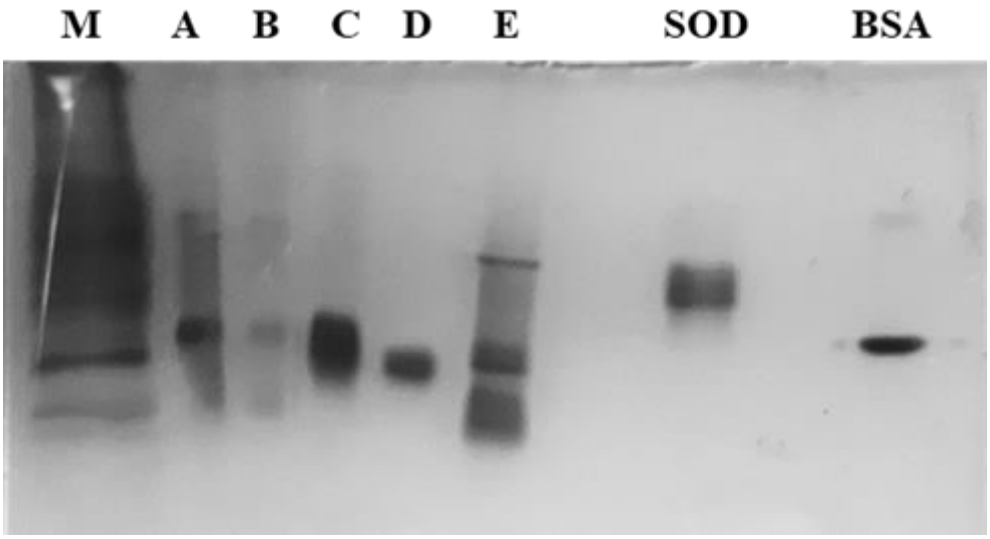

Figure 37 - **NATIVE-PAGE followed by Coomassie staining**. (M) markers, (A) *Korarchaeum cryptofilum* SOR supplemented with iron, (B) *Kc* SOR supplemented with iron and cobalt, (C) *Archaeoglobus fulgidus* SOR supplemented with iron, (D) *Archaeoglobus fulgidus* H46S mutant supplemented with cobalt; (E) *Korarchaeum cryptofilum* S70H mutant supplemented with iron, (SOD) superoxidase dismutase 5 µg; (BSA) 1 mg/mL bovine serum albumin.

To determine the identity of the bands observed in the NBT stained gel, the image was overlapped with the Coomassie stained gel image, which was run in the same conditions. The gel overlap confirms the activity associated to SOD and for the *Archaeoglobus fulgidus* SOR supplemented with iron, as well as some activity associated with *Af* H46S supplemented with cobalt. As for *Korarchaeum cryptofilum* SOR wild-type and mutant, no dismutase activity is observed.

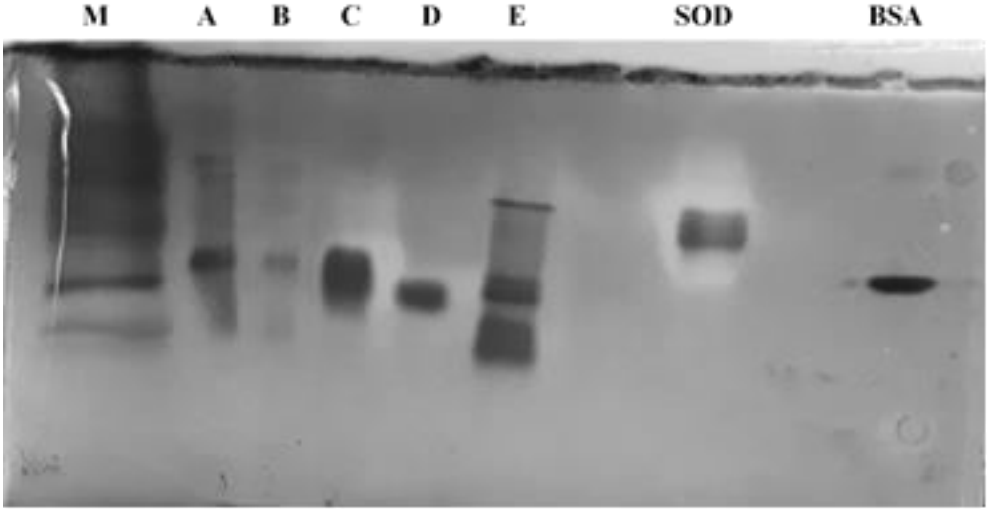

Figure 38 - Overlay NATIVE-PAGE followed by Nitrobluetetrazolium (fig 31) **and Coomassie** (fig 32) **staining**. (M) markers, (A) *Korarchaeum cryptofilum* SOR supplemented with iron, (B) *Kc* SOR supplemented with iron and cobalt, (C) *Archaeoglobus fulgidus* SOR supplemented with iron, (D) *Archaeoglobus fulgidus* H46S mutant, supplemented with cobalt; (E) *Korarchaeum cryptofilum* S70H mutant supplemented with iron, (SOD) superoxidase dismutase 5 µg; (BSA) 1 mg/mL bovine serum albumin. This overlay, confirms that the dismutase activity results from *Archaeoglobus fulgidus* SOR supplemented with iron (C) and superoxidase dismutase (SOD).

4.4.4. X-ray crystallography

4.4.4.1. *Korarchaeum cryptofilum* SOR crystallisation

Crystallisation screenings were carried out at the nano litter scale using a 12 mg/mL protein solution in 50 mM Tris-HCl pH 7.5 and 150 mM NaCl for structure screen 1&2 (Molecular Dimension) solutions, in a Mosquito LCP with iQ plates (TTP Lab) at room temperature and 4 ºC.

Urchin-like crystals appear in condition G3 (10 mM zinc sulfate heptahydrate, 100 mM MES pH 6.5, 25 % v/v PEG 500 MME) at room temperature. Further optimisation and scale-up of this condition were attempted without success.

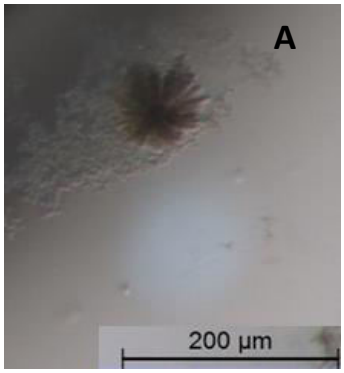

Figure 39 - *Korarchaeum cryptofilum* SOR supplemented with iron crystal, obtained with the initial structure screen 1&2, at room temperature. Urchin-like crystal condition #G3

Another crystallisation trial for *Korarchaeum cryptofilum* SOR was performed. However, in this case, prior to crystallisation trial, protein sample was loaded onto a size exclusion column, S75 (buffer 0.05 M Tris-HCl pH 7.5, 0.15 M NaCl), to exclude different oligomeric states (dimer and hexamer). Then, the structure screen 1&2 (Molecular Dimension) was tested using a mosquito LCP with iQ plates (TTO Lab) at 20 ºC and 4 ºC.

Crystal formation for the dimer oligomeric states was successful with the condition #B1 (Sodium citrate tribasic, 0.1 M sodium cacodylate pH 6.5, 30% v/v 2-propanol at 4 ºC in the ratio 2:1). From this batch, crystals were sent to DLS synchrotron (UK) but unfortunately no crystal diffracted.

4.4.4.2. *Archaeoglobus fulgidus* SOR H46S mutant crystallisation

For the *Archaeoglobus fulgidus* SOR H46S, supplemented with cobalt, crystallisation screens were setup at nL scale using 12 mg/mL protein solution in 0.05 M Tris-HCl pH 7.5. 0.15 M NaCl and structure screen 1&2 (Molecular Dimension) solutions, in a Mosquito LCP with iQ plates (TTP Lab) at 20 ºC. Some crystals appeared in 3 protein to precipitant ratios (1:1; 1:2; 2:1) in the condition #A9 (0.1 M Sodium citrate pH 5.6, 20% w/v PEG 4000) and condition #C9 (0.2 M magnesium chloride hexahydrate, 0.1 M Tris pH 8.5, 20% w/v PEG 4000).

Crystals from the condition #C9 were send to ALBA Synchrotron and diffracted at 3 Å. Given the low resolution, the condition #C9 was submitted to further optimisation: 2 µL (1:1) hanging drop in vapor diffusion with 500 µL reservoir solution, were the pH and %PEG vary in the crystallisation buffer. Better crystals were observed for the condition 0.2 M magnesium chloride hexahydrate, 0.1 M Tris pH 8, 27% w/v PEG 4000.

Afterwards, the Morpheus Additive Screen (Molecular Dimension) in a Mosquito LCP with iQ plates (TTP Lab) at 20 ºC, with the protein to precipitant ratio 1:1 was used, resulting in a great variety of crystals, like hexane/round/triangle-shape crystals which improved the crystals quality. From the additive screen 15 crystals were chosen and send in the ESRF trip. This trip resulted in data collection for two crystals obtained in the follow crystallisation conditions:

-**Crystal #1** - 0.2 M Magnesium chloride hexahydrate, 0.1 M Tris pH 8, 27% w/v PEG 4000, 3% w/v 1,8-Diaminooctane, 20% glycerol. (2.5 Å)

-**Crystal #2** - 0.2 M Magnesium chloride hexahydrate, 0.1 M Tris pH 8, 27% w/v PEG 4000, AMPD, 20% Glycerol. (2.6 Å)

The crystals were collected and were immediately flash cryo-cooled in liquid nitrogen.

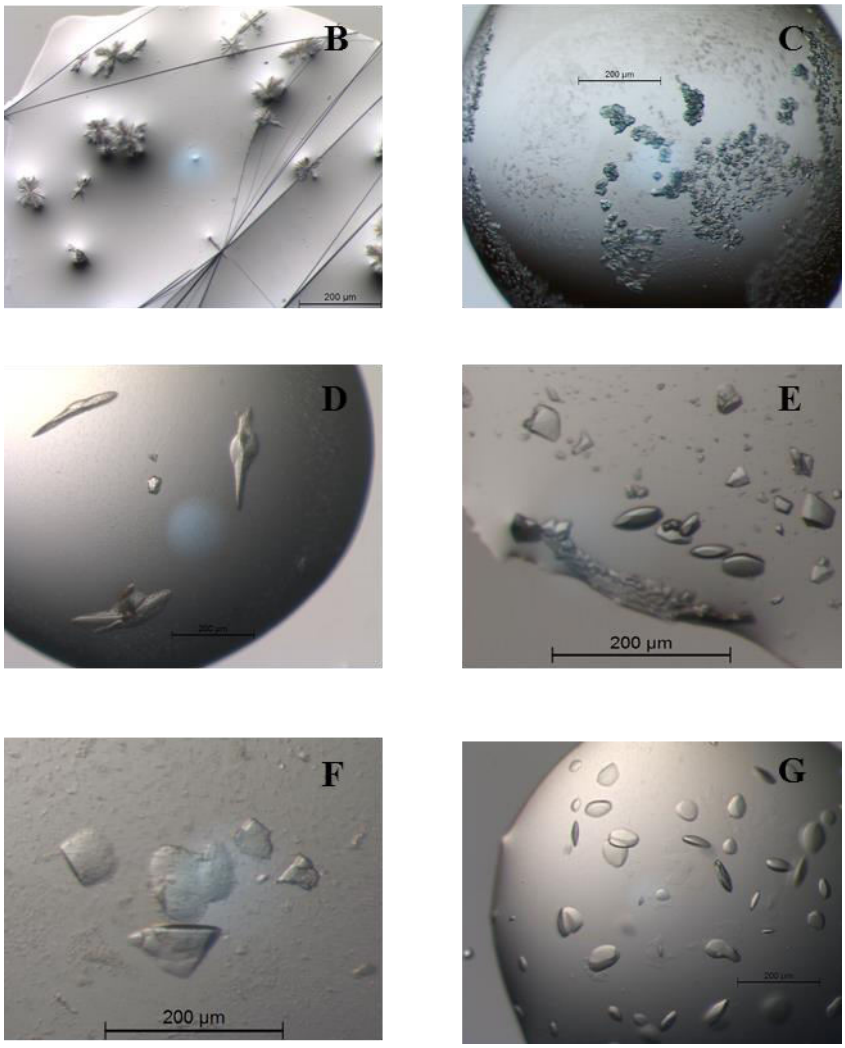

Figure 40 - X-ray crystallography, ***Archaeoglobus fulgidus*** **mutant, H46S supplemented with cobalt, crystals**. (B) Urchin-like crystal condition #A11 (0.5 M MES monohydrate), (C) Round-shape crystals conditions #E6, (D) prims-like crystals, #E6 additive condition #B4 (0.5 M Trizma® base buffer), (E) hexane-shape crystals condition, #E6 additive condition #C6 (0.4 M 1,6-Hexanediol), (F) Diamond-shape crystals, #E6 additive condition #F3 (0.05 M AMPD) (G) round-shape crystals, #E6 additive condition #E1 (0.4 M glycine).

4.4.4.3. Diffraction data collection and structure determination

Af H46S crystals were stored in liquid nitrogen and shipped to ESRF (Grenoble, France) where they were irradiated with X-rays and, in order to prevent radiation damage, all data collection was performed at 100 K. Diffraction images were obtained (Fig. 48) using the oscillation method and processed with XDS. MATTPROB was used to estimate the content of the unit cell and revealed the presence of two molecules in the asymmetric unit.

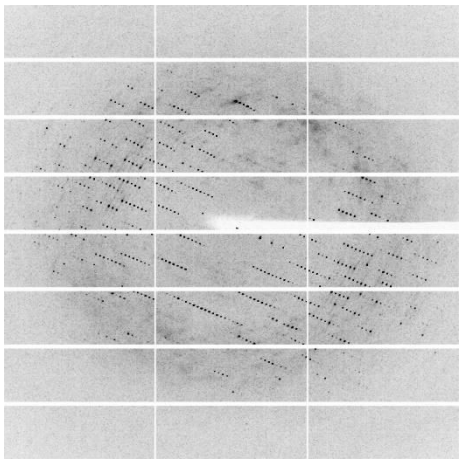

Figure 41 - Diffraction pattern of the *Archaeoglobus fulgidus* SOR mutant H46S, supplemented with cobalt. Resolution at the edge is 2.5 Å. The dataset was obtained at ESRF.

The structure of the *Archaeoglobus fulgidus* SOR (PDB - 4BGL) was used as a model to determine the structure of the mutant protein through molecular replacement (MR), after the starting phases were calculated using PHASER (PHENIX). PHENIX.REFINE was used in order to refine the structure, after examining 2m | Fo | -D | Fc | and m | Fo | -D | Fc | electron density maps with COOT. The presence of cobalt in the non-canonical centre II is clearly observable in the Fo-Fc map (Fig. 42).

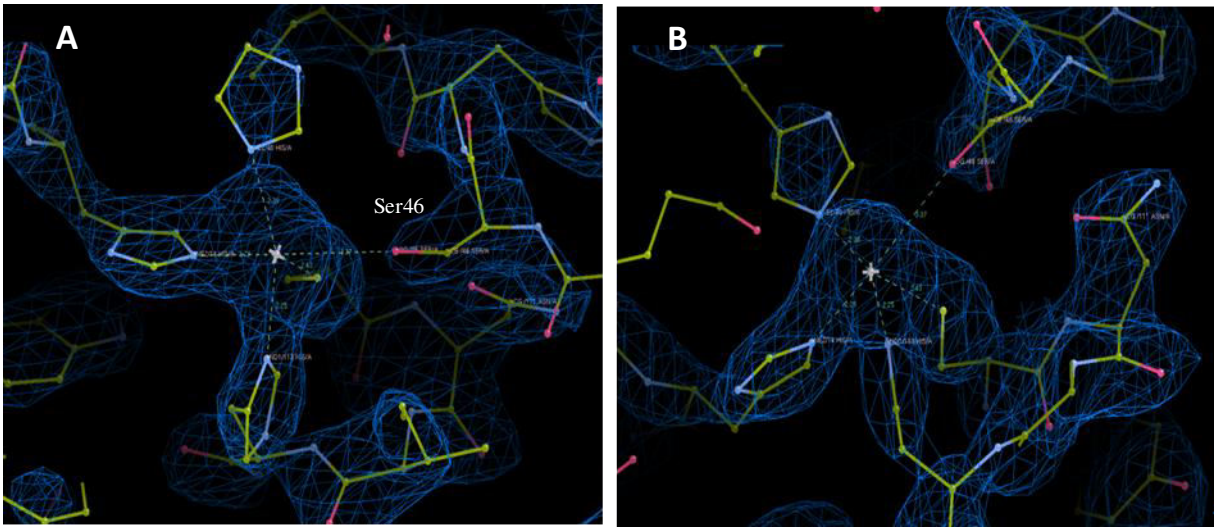

Figure 42 – Fo-Fc map of the non-canonical neelaredoxin centre. *Archaeoglobus fulgidus* mutant H46S supplemented with cobalt; (A) mutation localization, serine present in position 46 and (B) cobalt incorporated in the non-canonical catalytic centre II.

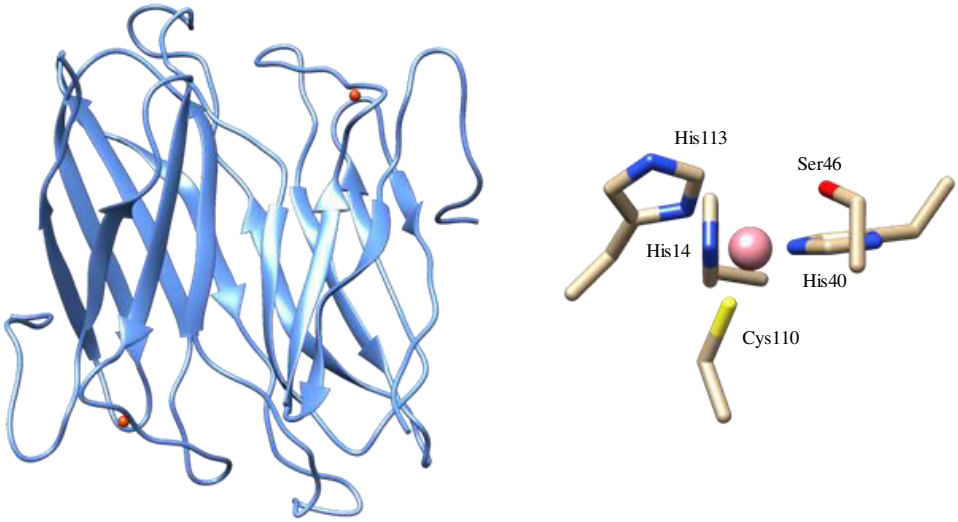

Figure 43 - Structure of the non-canonical neelaredoxin centre – (left) *Archaeoglobus fulgidus* mutant H46S supplemented with cobalt; (right) zoom-in of the non-canonical neelaredoxin centre; cobalt atoms are represented by pink spheres. The images were prepared with Chimera.

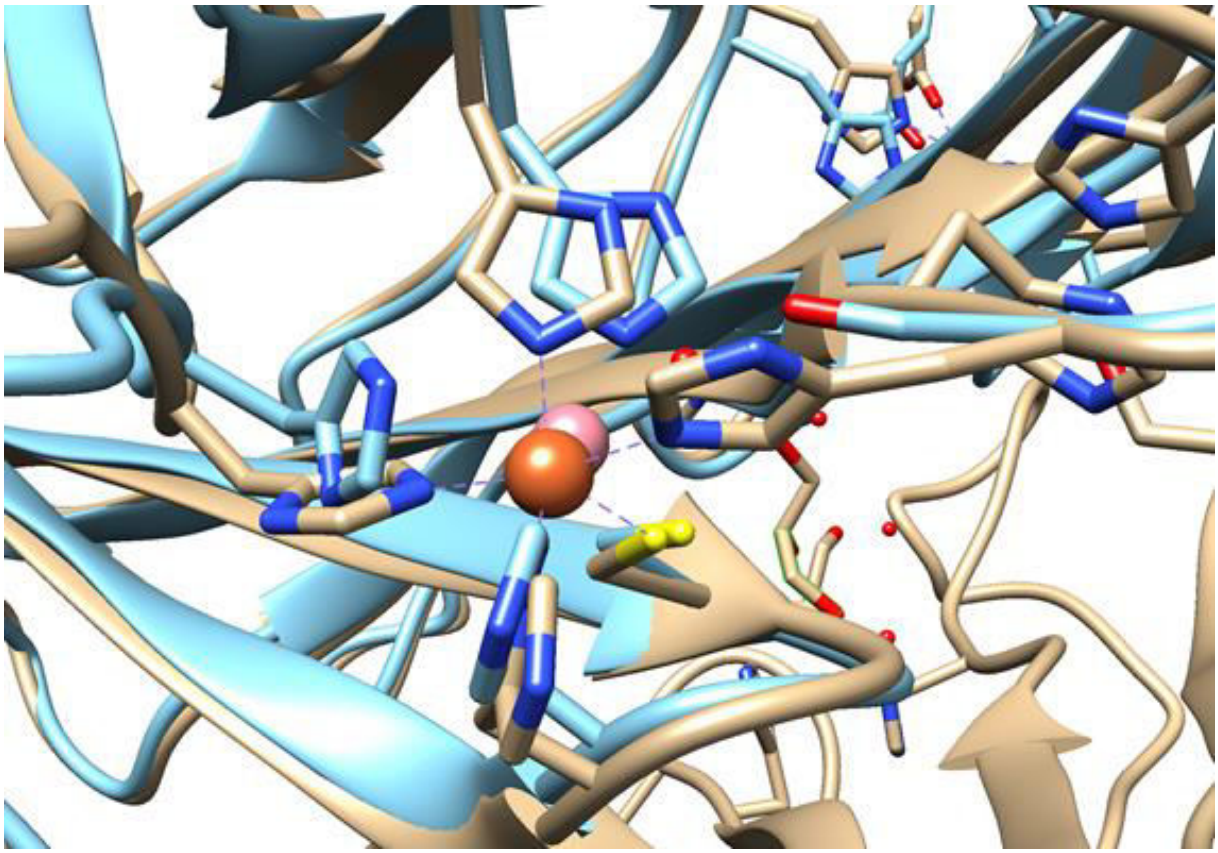

Figure 44 – Detail view of the neelaredoxin centre. Structural overlap of *Archaeoglobus fulgidus* SOR (brown polypeptide chain) with iron in the catalytic centre (red sphere) and H46S mutant (blue polypeptide chain) supplemented with cobalt (pink sphere). The images were prepared with PyMOL.

5. Discussion

The major goal of this thesis was to study a non-canonical superoxidase reductase which differed from the canonical ones, not only at the level of the ligands of the catalytic centre, but also by the presence of an extra domain at its C-terminus, and consequently the impact that these differences may have on the protein production and on its enzymatic activity.

Once the overexpression conditions were optimized, and the proteins were expressed and purified, the initial UV-visible analysis was performed. This analysis revealed spectroscopic differences between *Korarchaeum cryptofilum* SOR and canonical 2Fe-SORs (Fig. 45).

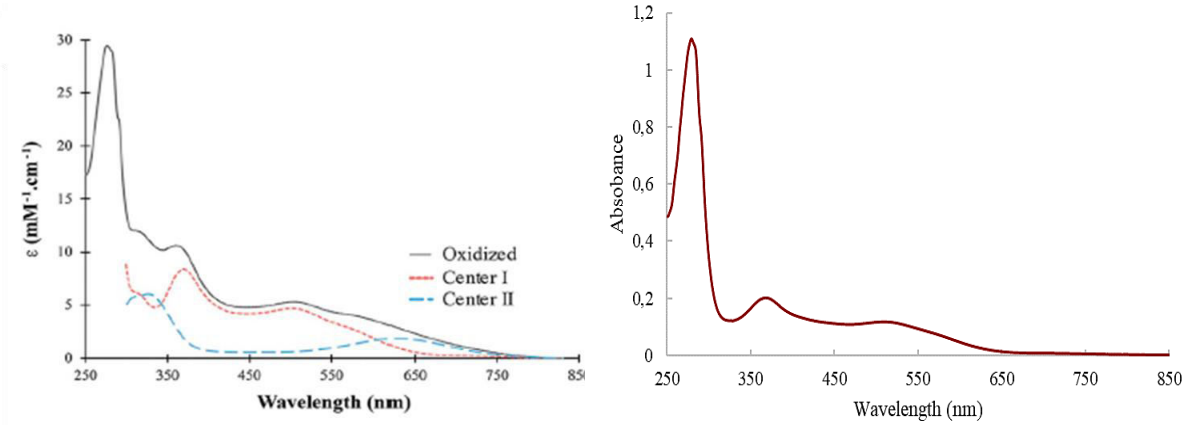

Figure 45 – Comparison between UV–Visible spectra of canonical 2Fe Sor and UV-Visible spectra of non-canonical 2Fe-SOR - *Korarchaeum cryptofilum* SOR. (Left) UV–visible spectra of 2Fe-SOR. 2Fe-SOR in the fully oxidised state (Fe^{3+}-Fe^{3+}) and the correspondent Centre I and Centre II components. Grey solid line represents the spectrum of the fully oxidised form; Pink dashed line represents the spectrum of the oxidised Centre I and the Blue dashed line the spectrum of the oxidised Centre II (from M. C. Martins et al 2019). (Right) UV-Visible spectrum of *Korarchaeum cryptofilum* SOR with Fe supplemented, as purified.

Even upon oxidation, the contribution of the centre II for the UV-Vis spectrum of *Kc* SOR was not observed, suggesting the absence of iron in the catalytic centre or the presence of a different metal, namely zinc, which would not contribute to the UV-Visible spectrum. The ability of SORs to bind different metals other than iron, like zinc, in its centres was already described in the literature.[79] This feature was also observed in both desulforedoxin and rubredoxin.[74] Besides the UV-Visible spectrum, the EPR also showed no evidence of the presence of iron in centre II (Fig. 32), demonstrating only the features characteristics of the centre I.

However, the metal quantifications by ICP-AES did not show the presence of zinc in the sample, which lead to the hypothesis that no other metal was present in centre II. These results were confirmed by the UV-Visible and EPR spectra of the *Af* H46S mutant, supplemented with iron, that mimics *Kc* centre II, which showed no spectroscopic feature similar to the WT *Af* SOR (Figures 29 and 35).

Therefore, expression of *Korarchaeum cryptofilum* SOR with different metals supplements such as copper, zinc and nickel were attempted to understand the ability of this protein to bind other metals than iron. In fact, an azurin mutant with a coordination similar to the *Kc* centre II, *i.e.*, three equatorial histidines and an axial cysteine residue, was described to bind both copper and cobalt.[76]

Overexpression with copper or zinc as supplements was not successful as there was no protein expression observed in the SDS-PAGE analysis. The supplementation with nickel resulted in protein expression but in very low amounts.

When compared with the literature the UV-visible data obtained for the *Kc* supplemented with iron and cobalt shows features consistent with a cobalt-bound centre.[80,81] However, by comparing with the spectroscopic data available in the literature for rubredoxin and desulforedoxin (metal centre coordinated by four cysteines)[74] and azurin M121H mutant (metal centre coordinated by three histidines and one cysteine),[76] it was not possible to determine in which centre the cobalt incorporation occurred. As for the iron supplemented protein, the EPR analysis of this sample did not reveal any feature of the presence of iron. Therefore, and in accordance with the UV-Visible spectrum, the EPR spectrum observed should be due to the presence of cobalt.

To verify the spectroscopic features of a SOR centre II with the coordination observed in *Kc* SOR, a site-directed mutant of a canonical 1Fe-SOR was used. In this case, a mutant of the *Archaeoglobus fulgidus* SOR,[16] which only possesses the neelaredoxin centre, *Af* H46S, was produced, in order to mimic the *Kc* SOR non-canonical neelaredoxin centre. The UV-Visible characterisation of the *Af* H46S, showed features that indicated cobalt incorporation (Figure 30). Similarly, the EPR spectrum of this sample also showed features attributable to a cobalt incorporated centre (Figure 34). On the other hand, the production of the wild-type *Af* SOR supplemented with cobalt was not able to incorporate this metal. Although similar, the spectroscopic features of the cobalt supplemented *Kc* SOR and *Af* H46S point to slight differences between the two samples (Figure 34). The differences between these two samples, together with the spectroscopic similarities found between the cobalt supplemented *Kc* SOR and cobalt substituted rubredoxin and desulforedoxin samples, indicates that the cobalt incorporation might have occurred in centre I and not centre II.

Another important fact to verify, was the influence of the *Kc* SOR extra domain in the C-terminal in metal incorporation in the centre II. To evaluate this hypothesis, a site-directed mutant was produced, S70H. This mutant returns the natural mutation of the *Kc* SOR centre II to a canonical one with four histidines and one cysteine. After an iron supplemented protein overexpression, this mutant presented similar spectroscopic characteristics with the wild-type *Kc* SOR supplemented with iron (Figures 31 and 35). These results indicate that no iron was present at centre II. This may indicate an influence of the extra domain in the ability of this protein to bind a metal ion at centre II.

To confirm this hypothesis, an attempt was made to solve the structure of *Kc* SOR by X-ray crystallography but, unfortunately, the crystals obtained were of insufficient diffraction quality. However, it was possible to obtain, the structure for the *Af* H46S supplemented with cobalt, showing cobalt incorporation (Fig. 46), coordinated by three equatorial histidines and an axial cysteine, like mutant azurin's case.[76] This is a very relevant result as the incorporation of cobalt in this protein represents a new type of coordination in a cobalt centre.

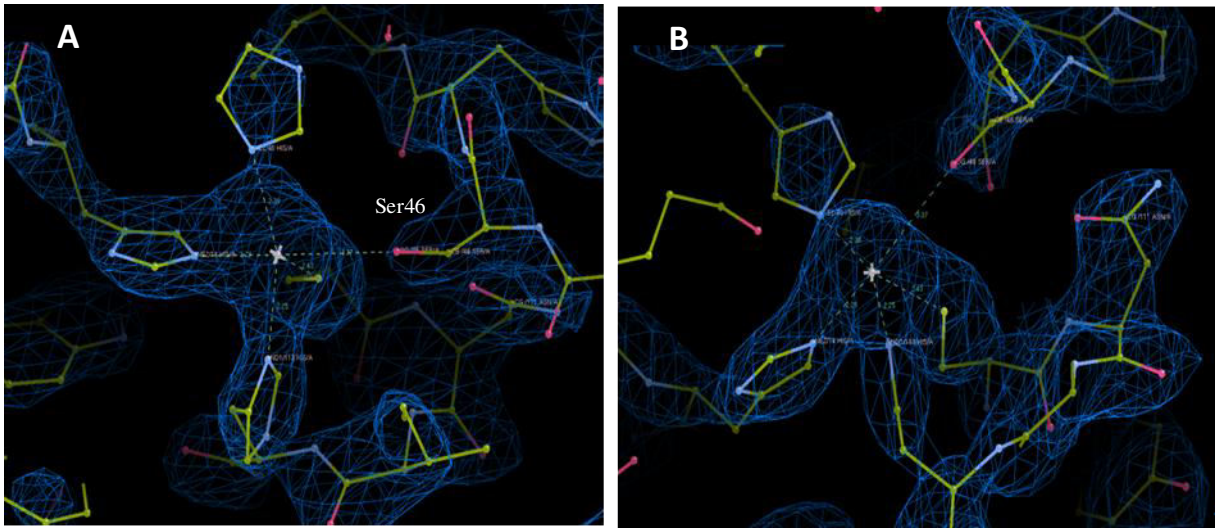

Figure 46 - Fo-Fc map of the non-canonical neelaredoxin centre. *Archaeoglobus fulgidus* mutant H46S supplemented with cobalt; (A) mutation localization, serine present in position 46 of amino acid sequence and (B) Cobalt incorporated in the non-canonical catalytic centre II.

Given the novelty of this type of catalytic centre in a SOR, it was important to evaluate its ability to perform the reaction with superoxide. As the redox partner of the *Kc* SOR is not known, a SOD assay in a native gel electrophoresis was performed with all the proteins produced. The native activity gel showed that neither *Korarchaeum cryptofilum* SOR or its mutant, S70H presented superoxidase dismutase activity, while the *Archaeoglobus fulgidus* SOR supplemented with iron, showed strong activity, as it was expected, similar to the SOD (positive control). On the other hand, both wild-type *Kc* SOR and *Af* mutant H46S supplemented with cobalt showed no SOD activity. Although the absence of SOD activity in *Kc* SOR may be related to the absence of metal (cobalt or iron) incorporation in the centre II, the absence of SOD activity in the cobalt supplemented *Af* H46S reveals that this protein may have a different substrate than superoxide.

6. Conclusion

This thesis focused on the study of a superoxide reductase (SOR) of *Candidatus Korarchaeum cryptofilum,* which has a non-canonical catalytic centre. Throughout this work, the superoxide dismutase activity of this enzyme was not observed.

Incorporation of iron, the characteristic SOR cofactor, was not detected in the neelaredoxin centre, whether for the wild type enzyme with the non-canonical centre II or mutant proteins, with the canonical centre, being only detected in the desulforedoxin centre. Moreover, a canonical SOR mutated to have a similar centre to *Kc* SOR was also unable to bind iron. This suggests that the coordination of this non-canonical neelaredoxin centre is uncapable of iron incorporation.

Besides iron, *Kc* SOR was also unable to bind copper, zinc, or nickel into the non-canonical centre II. As for cobalt, the ICP-AES determination, EPR analysis and comparison between UV-visible data acquired and the literature for cobalt-substituted rubredoxin and desulforedoxin, it was possible to confirm that cobalt incorporation occurred but not its location (centre I or Centre II). Although the similarities between the *Kc* SOR with cobalt and rubredoxin and desulforedoxin (cobalt substituted) point to its incorporation in centre I. Moreover, the NATIVE-PAGE SOD assay results, showed no dismutase activity for the *Kc* SOR which could be explain either by the absence of metal in the neelaredoxin centre or by a different substrate than superoxide for the cobalt enzyme.

Similarly, the *Af* H46S mutant, with a centre similar to *Kc* SOR was also able to incorporate cobalt in the non-canonical centre II as confirmed by ICP-AES quantification and UV-visible and EPR spectroscopies, however it was also unable to use superoxide, which corroborate the possibility of a different substrate for the non-canonical centre. The three-dimensional structure determined for this Co-substituted SOR revealed a novel typo of cobalt coordination in a protein- the cobalt is bound to three histidines and a cysteines, in a distort-ed tetrahedral geometry.

Finally, and besides what was mentioned above, the spectroscopic features of the *Kc* S70H mutant, which restored the canonical catalytic center, showed that this protein was also unable to bind iron in center II. These results also point to the possibility that the extra domain creates a structural impediment to metal incorporation, regardless of the centre being canonical or non-canonical.

Further studies, namely a different *Kc* SOR mutant without the C-terminal extra domain are needed to elucidate, not only the role of this extra domain, but also the enzymatic activity of this protein.

7. References

1. Sessions, A. L., Doughty, D. M., Welander, P. V., Summons, R. E. & Newman, D. K. The Continuing Puzzle of the Great Oxidation Event. *Current Biology* vol. 19 (2009).
2. Raymond, J. & Segrè, D. The effect of oxygen on biochemical networks and the evolution of complex life. *Science (80-.).* 311, 1764–1767 (2006).
3. Dahlgren, C. & Karlsson, A. Respiratory burst in human neutrophils. *J. Immunol. Methods* 232, 3–14 (1999).
4. Lu, Y. *et al.* Construction of a "Blue" Copper Site at the Native Zinc Site of Yeast Copper-Zinc Superoxide Dismutase. *J. Am. Chem. Soc.* 115, 5907–5918 (1993).
5. Mittal, M., Siddiqui, M. R., Tran, K., Reddy, S. P. & Malik, A. B. Reactive oxygen species in inflammation and tissue injury. *Antioxidants and Redox Signaling* vol. 20 1126–1167 (2014).
6. Liguori, I. *et al.* Oxidative stress, aging, and diseases. *Clin. Interv. Aging* Volume 13, 757–772 (2018).
7. Stadtman, E. R. & Levine, R. L. Protein oxidation. in *Annals of the New York Academy of Sciences* vol. 899 191–208 (New York Academy of Sciences, 2000).
8. Ylä-Herttuala, S. Oxidised LDL and atherogenesis. in *Annals of the New York Academy of Sciences* vol. 874 134–137 (New York Academy of Sciences, 1999).
9. Marnett, L. J. Oxyradicals and DNA damage. *Carcinogenesis* 21, 361–370 (2000).
10. Kiss, P. J. *et al.* Inactivation of NADPH oxidase organizer 1 results in severe imbalance. *Curr. Biol.* 16, 208–213 (2006).
11. Robinett, N. G., Peterson, R. L. & Culotta, V. C. Eukaryotic copper-only superoxide dismutases (SODs): A new class of SOD enzymes and SOD-like protein domains. *Journal of Biological Chemistry* vol. 293 4636–4643 (2018).
12. Sheng, Y. *et al.* Superoxide dismutases and superoxide reductases. *Chem. Rev.* 114, 3854–3918 (2014).
13. Moura, I. *et al.* Purification and characterisation of desulfoferrodoxin. A novel protein from *Desulfovibrio desulfuricans* (ATCC 27774) and from *Desulfovibrio vulgaris* (strain Hildenborough) that contains a distorted rubredoxin centre and a mononuclear ferrous centre. *J. Biol. Chem.* 265, 21596–21602 (1990).
14. Moura, I., Bruschi, M., Le Gall, J., Moura, J. J. G. & Xavier, A. V. Isolation and characterisation of desulforedoxin, a new type of non-heme iron protein from *Desulfovibrio gigas. Biochem. Biophys. Res. Commun.* 75, 1037–1044 (1977).
15. Bult, C. J. *et al.* Complete genome sequence of the Methanogenic *archaeon, Methanococcus jannaschii. Science (80-.).* 273, 1058–1073 (1996).
16. Klenk, H. P. *et al.* The complete genome sequence of the hyperthermophilic, sulphate-reducing a*rchaeon Archaeoglobus fulgidus*. *Nature* 390, 364–370 (1997).
17. Kawarabayasi, Y. *et al.* Complete sequence and gene organization of the genome of a hyper-thermophilic *archaebacterium, Pyrococcus horikoshii* OT3. *DNA Res.* 5, 55–76 (1998).
18. Nelson, K. E. *et al.* Evidence for lateral gene transfer between *archaea* and bacteria from genome sequence of *Thermotoga maritima. Nature* 399, 323–329 (1999).
19. Jenney, F. E., Verhagen, M. F. J. M., Cui, X. & Adams, M. W. W. Anaerobic microbes: Oxygen detoxification without superoxide dismutase. *Science (80-.).* 286, 306–309 (1999).
20. Lombard, M., Fontecave, M., Touati, D. & Nivière, V. Reaction of the desulfoferrodoxin from *Desulfoarculus baarsii* with superoxide anion. Evidence for a superoxide reductase activity. *J. Biol. Chem.* 275, 115–121 (2000).
21. Lombard, M., Touati, D., Fontecave, M. & Nivière, V. Superoxide Reductase as a Unique Defense System against Superoxide Stress in the *Microaerophile Treponema pallidum*. *J. Biol. Chem.* 275, 27021–27026 (2000).
22. Lucchetti-Miganeh, C., Goudenège, D., Thybert, D., Salbert, G. & Barloy-Hubler, F. SORGOdb: Superoxide reductase gene ontology curated dataBase. *BMC Microbiol.* 11, 1–12 (2011).
23. Emerson, J. P., Cabelli, D. E. & Kurtz, D. M. An engineered two-iron superoxide reductase lacking the [Fe(SCys)4] site retains its catalytic properties in vitro and in vivo. *Proc. Natl.*

Acad. Sci. U. S. A. 100, 3802–3807 (2003).
24. Yeh, A. P., Hu, Y., Jenney, F. E., Adams, M. W. W. & Rees, D. C. Structures of the superoxide reductase from *Pyrococcus furiosus* in the oxidised and reduced states. *Biochemistry* 39, 2499–2508 (2000).
25. Abreu, I. A. *et al.* Oxygen detoxification in the strict anaerobic *archaeon Archaeoglobus fulgidus*: superoxide scavenging by Neelaredoxin. *Mol. Microbiol.* 38, 322–334 (2000).
26. Rodrigues, J. V., Abreu, I. A., Cabelli, D. & Teixeira, M. Superoxide reduction mechanism of *Archaeoglobus fulgidus* one-iron superoxide reductase. *Biochemistry* 45, 9266–9278 (2006).
27. Santos-Silva, T. *et al.* The first crystal structure of class III superoxide reductase from *Treponema pallidum*. *J. Biol. Inorg. Chem.* 11, 548–558 (2006).
28. A.V. Coelho, P. Matias, V. Fulõp, A. Thompson, A. Gonzalez, M. A. C. Desulfoferrodoxin structure determined by the MAD phasing.pdf. 680–689 (1997).
29. Katona, G. *et al.* Raman-Assisted Crystallography. *Science (80-.).* 316, 449–453 (2007).
30. Adam, V., Royant, A., Nivière, V., Molina-Heredia, F. P. & Bourgeois, D. Structure of Superoxide Reductase Bound to Ferrocyanide and Active Site Expansion upon X-Ray-Induced Photo-Reduction. *Structure* 12, 1729–1740 (2004).
31. Silva, G., LeGall, J., Xavier, A. V., Teixeira, M. & Rodrigues-Pousada, C. Molecular characterisation of *Desulfovibrio gigas* neelaredoxin, a protein involved in oxygen detoxification in anaerobes. *J. Bacteriol.* 183, 4413–4420 (2001).
32. Mathé, C. *et al.* Identification of iron(III) peroxo species in the active site of the superoxide reductase SOR from *Desulfoarculus baarsii*. *J. Am. Chem. Soc.* 124, 4966–4967 (2002).
33. David, R., Jamet, H., Nivière, V., Moreau, Y. & Milet, A. Iron Hydroperoxide Intermediate in Superoxide Reductase: Protonation or Dissociation First? MM Dynamics and QM/MM Metadynamics Study. *J. Chem. Theory Comput.* 13, 2987–3004 (2017).
34. Pinto, A. F. *et al.* Superoxide reduction by a superoxide reductase lacking the highly conserved lysine residue. *J. Biol. Inorg. Chem.* 20, 155–164 (2015).
35. Clay, M. D. *et al.* Spectroscopic studies of *Pyrococcus furiosus* superoxide reductase: Implications for active-site structures and the catalytic mechanism. *J. Am. Chem. Soc.* 124, 788–805 (2002).
36. Mathé, C., Nivière, V. & Mattioli, T. A. Fe3+-hydroxide ligation in the superoxide reductase from *desulfoarculus baarsii* is associated with pH dependent spectral changes. *J. Am. Chem. Soc.* 127, 16436–16441 (2005).
37. Todorovic, S. *et al.* Resonance Raman study of the superoxide reductase from *Archaeoglobus fulgidus*, E12 mutants and a 'natural variant'. *Phys. Chem. Chem. Phys.* 11, 1809–1815 (2009).
38. Berthomieu, C., Dupeyrat, F., Fontecave, M., Verméglio, A. & Nivière, V. Redox-dependent structural changes in the superoxide reductase from *Desulfoarculus baarsii* and *Treponema pallidum*: A FTIR study. *Biochemistry* 41, 10360–10368 (2002).
39. Nivière, V. *et al.* Superoxide Reductase from *Desulfoarculus baarsii:* Identification of Protonation Steps in the Enzymatic Mechanism. *Biochemistry* 43, 808–818 (2004).
40. Abreu, I. A., Saraiva, L. M., Soares, C. M., Teixeira, M. & Cabelli, D. E. The Mechanism of Superoxide Scavenging by *Archaeoglobus fulgidus* Neelaredoxin. *J. Biol. Chem.* 276, 38995–39001 (2001).
41. Emerson, J. P., Coulter, E. D., Cabelli, D. E., Phillips, R. S. & Kurtz, D. M. Kinetics and mechanism of superoxide reduction by two-iron superoxide reductase from *Desulfovibrio vulgaris*. *Biochemistry* 41, 4348–4357 (2002).
42. Nivière, V., Lombard, M., Fontecave, M. & Houée-Levin, C. Pulse radiolysis studies on superoxide reductase from *Treponema pallidum*. *FEBS Lett.* 497, 171–173 (2001).
43. Lombard, M., Houée-Levin, C., Touati, D., Fontecave, M. & Nivière, V. Superoxide reductase from *Desulfoarculus baarsii*: Reaction mechanism and role of glutamate 47 and lysine 48 in catalysis. *Biochemistry* 40, 5032–5040 (2001).
44. Dey, A. *et al.* Sulfur K-edge X-ray absorption spectroscopy and density functional theory calculations on superoxide reductase: Role of the axial thiolate in reactivity. *J. Am. Chem. Soc.* 129, 12418–12431 (2007).
45. Silaghi-Dumitrescu, R. *et al.* A flavodiiron protein and high molecular weight rubredoxin from *Moorella thermoacetica* with nitric oxide reductase activity. *Biochemistry* 42, 2806–2815

(2003).
46. Meyer, J. & Moulis, J.-M. Rubredoxin. in *Handbook of Metalloproteins* (John Wiley & Sons, Ltd, 2006). doi:10.1002/0470028637.met135.
47. Grunden, A. M. *et al.* In vitro reconstitution of an NADPH-dependent superoxide reduction pathway from *Pyrococcus furiosus*. *Appl. Environ. Microbiol.* 71, 1522–1530 (2005).
48. Ma, K. & Adams, M. W. W. A hyperactive NAD(P)H:rubredoxin oxidoreductase from the hyperthermophilic *archaeon Pyrococcus furiosus*. *J. Bacteriol.* 181, 5530–5533 (1999).
49. Barns, S. M., Fundyga, R. E., Jeffries, M. W. & Pace, N. R. Remarkable archaeal diversity detected in a Yellowstone National Park hot spring environment. *Proc. Natl. Acad. Sci. U. S. A.* 91, 1609–1613 (1994).
50. Takai, K. & Horikoshi, K. *Genetic Diversity of Archaea in Deep-Sea Hydrothermal Vent Environments*. (1999).
51. Hjorleifsdottir, S., Skirnisdottir, S., Hreggvidsson, G. O., Holst, O. & Kristjansson, J. K. Species composition of cultivated and noncultivated bacteria from short filaments in an icelandic hot spring at 88°C. *Microb. Ecol.* 42, 117–125 (2001).
52. Elkins, J. G. *et al. A korarchaeal* genome reveals insights into the evolution of the *Archaea*. *Proc. Natl. Acad. Sci. U. S. A.* 105, 8102–8107 (2008).
53. Kobayashi, M. & Shimizu, S. Cobalt proteins. *Eur. J. Biochem.* 261, 1–9 (1999).
54. GRARD, T. *et al.* Soluble forms of α-d-mannosidases from rat liver: Separation and characterisation of two enzymic forms with different substrate specificities. *Eur. J. Biochem.* 223, 99–106 (1994).
55. Vallee, W. M. B. L. Cobalt as Probe and Label of Proteins. *Methods Enzymol.* 226, 52–71 (1993).
56. Rao, R. R. & Lawson, C. L. Structure of catabolite activator protein with cobalt(II) and sulfate. *Acta Crystallogr. Sect. FStructural Biol. Commun.* 70, 560–563 (2014).
57. Simonsen, L. O., Harbak, H. & Bennekou, P. Cobalt metabolism and toxicology-A brief update. *Science of the Total Environment* vol. 432 210–215 (2012).
58. Brylinski, M. & Skolnick, J. FINDSITE-metal: Integrating evolutionary information and machine learning for structure-based metal-binding site prediction at the proteome level. *Proteins Struct. Funct. Bioinforma.* 79, 735–751 (2011).
59. Khrustalev, V. V. *et al.* Cobalt(ii) cation binding by proteins. *Metallomics* 11, 1743–1752 (2019).
60. Hourai, S., Miki, M., Takashima, Y., Mitsuda, S. & Yanagi, K. Crystal structure of nitrile hydratase from a *thermophilic Bacillus* smithii. *Biochem. Biophys. Res. Commun.* 312, 340–345 (2003).
61. Du, X., Tove, S., Kast-Hutcheson, K. & Grunden, A. M. Characterisation of the dinuclear metal centre of *Pyrococcus furiosus* prolidase by analysis of targeted mutants. *FEBS Lett.* 579, 6140–6146 (2005).
62. Tahirov, T. H. *et al.* Crystal structure of methionine aminopeptidase from hyperthermophile, *Pyrococcus furiosus*. *J. Mol. Biol.* 284, 101–124 (1998).
63. Ren, B., Tibbelin, G., Kajino, T., Asami, O. & Ladenstein, R. The multi-layered structure of Dps with a novel di-nuclear ferroxidase centre. *J. Mol. Biol.* 329, 467–477 (2003).
64. Kauko, A., Haataja, S., Pulliainen, A. T., Finne, J. & Papageorgiou, A. C. Crystal structure of Streptococcus suis Dps-like peroxide resistance protein Dpr: Implications for iron incorporation. *J. Mol. Biol.* 338, 547–558 (2004).
65. Kim, S. G., Bhattacharyya, G., Grove, A. & Lee, Y. H. Crystal Structure of Dps-1, a Functionally Distinct Dps Protein from *Deinococcus radiodurans*. *J. Mol. Biol.* 361, 105–114 (2006).
66. Haikarainen, T. *et al.* Structural and thermodynamic characterisation of metal ion binding in Streptococcus suis Dpr. *J. Mol. Biol.* 405, 448–460 (2011).
67. Gunčar, G. *et al.* The use of Co2+ for crystallisation and structure determination, using a conventional mono-chromatic X-ray source, of flax rust avirulence protein. *Acta Crystallogr. Sect. F Struct. Biol. Cryst. Commun.* 63, 209–213 (2007).
68. Rimsa, V., Eadsforth, T. & Hunter, W. N. The role of Co2+ in the crystallisation of human SENP1 and comments on the limitations of automated refinement protocols. *Acta Crystallogr.*

Sect. F Struct. Biol. Cryst. Commun. 67, 442–445 (2011).
69. *Sambrook, J., Fritsch, E. R., & Maniatis, T. (1989). Molecular Cloning: A Laboratory Manual (2nd ed.). Cold Spring Harbor, NY: Cold Spring Harbor Laboratory Press.*
70. Bradford, M. M. A rapid and sensitive method for the quantitation of microgram quantities of protein utilizing the principle of protein-dye binding. *Anal. Biochem.* 72, 248–254 (1976).
71. Ryu, W. S. *Molecular Virology of Human Pathogenic Viruses - Wang-Shick Ryu - Google Books*. (2017).
72. Gavel, O. Y. *et al.* A new type of metal-binding site in cobalt- and zinc-containing adenylate kinases isolated from sulfate-reducers *Desulfovibrio gigas* and *Desulfovibrio desulfuricans* ATCC 27774. *J. Inorg. Biochem.* 102, 1380–1395 (2008).
73. Mark J. Winter. *d-Block chemistry*. (Oxford University Press, 1994).
74. Moura, I., Teixeira, M., Moura, J. J. G. & LeGall, J. Spectroscopic studies of cobalt and nickel substituted rubredoxin and desulforedoxin. *J. Inorg. Biochem.* 44, 127–139 (1991).
75. Rodrigues, J. V., Saraiva, L. M., Abreu, I. A., Teixeira, M. & Cabelli, D. E. Superoxide reduction by *Archaeoglobus fulgidus* desulfoferrodoxin: Comparison with neelaredoxin. *J. Biol. Inorg. Chem.* 12, 248–256 (2007).
76. Salgado, J., Kroes, S. J., Berg, A., Moratal, J. M. & Canters, G. W. The dynamic properties of the M121H azurin metal site as studied by NMR of the paramagnetic Cu(II) and Co(II) metalloderivatives. *J. Biol. Chem.* 273, 177–185 (1998).
77. Moura. EPR and Mossbauer studies of desulforedoxin from <i>*Desulfovibrio gigas*</i> *Ciênc. Biol. (Portugal)* 5, (1980).
78. Tavares, P. *et al.* Spectroscopic properties of desulfoferrodoxin from *Desulfovibrio desulfuricans* (ATCC 27774). *J. Biol. Chem.* 269, 10504–10510 (1994).
79. Folgosa, F. *et al.* New spectroscopic and electrochemical insights on a class I superoxide reductase: evidence for an intramolecular electron-transfer pathway. *Biochem. J.* 438, 485–494 (2011).
80. Karlsson, B. G. *et al. Cassette mutagenesis of Metl21 in azurin from Pseudomonas aeruginosa*. *Protein Engineering vol* vol. 4 https://academic.oup.com/peds/article/4/3/343/1486661 (1991).
81. McMillin, D. R., Rosenberg, R. C. & Gray, H. B. Preparation and spectroscopic studies of cobalt(II) derivatives of blue copper proteins. *Proc. Natl. Acad. Sci. U. S. A.* 71, 4760–4762 (1974).

8. Appendix

Appendix 1 - Solutions composition

Reagent	Mass/Volume	Reagent	Mass/Volume
Liquid LB		**M9 medium***	
Triptone	10 g	M9 Salts (5x)	200 mL
Yeast Extract	5 g	1 M $MgSO_4$	2 mL
NaCl	10 g	5 M $CaCl_2$	0.020 mL
H_2O Milli-Q	Up to 1000 mL	1 M Glucose	20 mL
		0.1 M Metal supplement	2 x 1 mL
LB agar		Kanamycin (50 mg/mL)	1 mL
Triptone	5 g	H_2O Milli-Q	up to 750 mL
Yeast Extract	2.5 g	0.1 M IPTG	0.1 mL
NaCl	5 g	Pre-inocolum	30 mL
Agar	10 g	*For one erlenmeyer, up to 8	
H_2O Milli-Q	Up to 1000 mL		
M9 Salts		**Supplement $FeCl_2$ (0.1 M)**	
$Na_2HPO_4.7H_2O$	128 g	$FeCl_2$	0.99 g
KH_2PO_4	30 g	H_2O Milli-Q	50 mL
NH_4Cl	10 g		
NaCl	5 g	**Supplement $CoSO_4$ (0.1 M)**	
H_2O Milli-Q	Up to 2000 mL	$CoSO_4$ (M = 154.996 g/mol)	0.47 g
		H_2O Milli-Q	50 mL
Buffer Solution Tris-HCl 1M			
Tris base	121.14 g	**Supplement $NiCl_2$ (0.1 M)**	
HCl (8M)	until pH = 7,5	$NiCl_2$ (M = 237.69 g/mol)	0.51 g
distilled H_2O	up to 1000 mL	H_2O Milli-Q	50 mL

Appendix 3 - Buffer Solutions composition

Buffer Solution A	Volume	Buffer Solution C	Volume
1M Tris-HCl pH 7.5	40 mL	1M Tris-HCl pH 7.5	40 mL
Glycerol	100 mL	NaCl (4M)	75 mL
H_2O Milli-Q	Up to 2000 mL	Glycerol	100 mL
		H_2O Milli-Q	Up to 2000 mL
Buffer Solution B			
1M Tris-HCl pH 7.5	20 mL	**Buffer Solution Dialysis**	
Glycerol	50 mL	1M Tris-HCl pH 7.5	100 mL
NaCl (4M)	250 mL	Glycerol	250 mL
H_2O Milli-Q	Up to 1000 mL	distilled H_2O	Up to 5000 mL

Appendix 3 – Transformation protocol

The transformation protocol used throughout this work was slightly adapted from NZYtech® protocol.

The BL21(DE3) chemically competent *Escherichia coli* cells used were stored at -80 °C.

Competent cells control plasmid solution (0.1 ng/µL) is provided as a control to determine the transformation efficiency. To obtain maximum transformation efficiency, the experimental DNA must be free of phenol, ethanol, protein and detergents.

1. Thaw competent cells on ice. Gently mix cells. Do not mix cells by pipetting.

2. In 2 separate microcentrifuge tubes, add 50 µL of BL21(DE3) Competent Cells, one is used as positive control and the other for the protein over expression.

3. Add 2 µL of the plasmid DNA to the protein over expression microcentrifuge tubes.

4. Incubate cells on ice for 30 minutes.

5. Heat-shock cells for 30 seconds in a 42 °C water bath; do not shake.

6. Place on ice for 2 minutes.

7. Add 900 µL room temperature LB medium.

8. Shake at 150 rpm (37 °C) for 90 mins.

9. On 3 different LB agar plates containing kanamycin, 1- spread 100 µL of cells transformed with competent cells with DNA plasmid; 2 - spread 200 µL of cells transformed with competent cells with DNA plasmid; 3 - spread 200 µL of cells transformed with competent cells without DNA plasmid.

11. Incubate overnight at 37 °C.

Appendix 4 – Miniprep protocol NZYtech

The miniprep protocol used in this work was the NZYSpeedy Miniprep from NZYtech®

Protocol for plasmid DNA purification from *Escherichia coli* cells.

All centrifugations should be carried out at room temperature in a table-top microcentrifuge at >12000 xg (10000-15000 rpm depending on the rotor type).

1. Cultivate and harvest bacterial cells

Pellet 1-5 mL of an *E. coli* LB culture for 30 s. Discard supernatant. Remove as much media as possible.

2. Cell lysis

Re-suspend cell pellet completely in 250 µL of Buffer A1 by vigorous vortexing/pipetting. Add 250 µL of Buffer A2 and mix gently by inverting the tube for 5 times. Incubate at room temperature (10-25 ºC) for up to 2 min. Do not vortex. Add 300 µL of Buffer A3. Mix gently by inverting the tube for 6-8 times. Do not vortex.

3. Clarification of lysate

Centrifuge for 3 min (13 000 rpm) at room temperature to pellet precipitate.

4. Bind DNA

Place Nzytech spin column in a 2 mL collecting tube and load the supernatant from step 3 onto the column. Centrifuge for 1 min at 11 000 xg. Discard flow-through.

5. Wash silica membrane

Add 500 µL of Buffer AY onto the column. Centrifuge for 1 min. Discard flow-through. Add 400 µL of Buffer A4 (make sure ethanol was previously added). Centrifuge for 1 min. Discard flow-through.

6. Dry silica membrane

Re-insert the Nzytech spin column into the empty 2 mL collecting tube and centrifuge for 2 min.

7. Elute highly pure DNA

Place the dried Nzytech spin column into a clean 1.5 mL microcentrifuge tube and add 50 µL of PCR H_2O. Incubate for 1 min at room temperature (10-25 ºC). Centrifuge for 1 min. By repeating this step the overall yield will increase by 15-20%. To obtain a highly concentrated miniprep (1.3 times higher) reduce the volume of elution buffer to 30 µL. Store the purified DNA at -20 °C.

Appendix 5 – Bradford protein assay protocol

To determine protein concentration the Bradford protein assay method was used. This method uses BSA protein to determine a calibration curve (0.5 mg/ml).

V (BSA Standard) / µL	V (H_2O) / µL	V (SOR 1:10) / µL
0	100	**3**
2.5	97.5	**3**
5	95	**5**
7.5	92.5	**5**
10	90	
15	85	
20	80	

It is necessary for the wavelength of protein in study, to stay in the wavelength break corresponding to the calibration curve.

After the preparation of the samples for the calibration curve and for the protein under study, 1 mL of Bradford reagent was added (1:5 from the stock) to each microcentrifuge tube and mixed with a vortex. The mixture was incubated at room temperature for 10 min and the absorbance was measure at 595 nm.

By making use of the calibration curve with the quantity of BSA (y= mx + b), protein concentration was determined in the follow steps:

a) Protein concentration mg/ml is determined with:

$$[\text{protein}]_{mg/ml} = ((\text{Abs } 595nm - b)/m/v_{[protein]}) * \text{dilution}_{\text{(if appliable)}}. \quad 7.1)$$

b) Median is acquired from all the $[\text{protein}]_{mg/ml}$ determined.

c) Final concentration is calculated:

$$[\text{protein}]_{nm} = (\text{median} / \text{Molecular mass}) * 1000. \quad 7.2)$$

Appendix 6 – Quaternary structure determination - Gel filtration

Peaks	Mass (Da)	Log (MM)	V (elution)/mL	MM	Quaternary Structure
Blue Dextran	2000000	6.3	8.7		
Tyroglobulin. bovine	669000	5.8			
Apoferritin	443000	5.7			
β-Amylase. sweet patato	200000	5.3			
Alcohol Dehydrogenase. yeast	150000	5.2			
Albumin. bovine serum	66000	4.8			
Carbonic Anhydrase. bovine Erythrocytes	29000	4.5			
***Kc* SOR Fe 1st peak**	25195	5.2	12.6	147373.7	5.8
***Kc* SOR Fe 2nd peak**	25195	4.8	14.7	58437.3	2.3